displays extraordinarily large fluctuations and will be discussed separately in Chapter 6. Note that all these shifts are commensurate with $L = 72$.

4.1. Methodologies

For the studies in this chapter, the overall density is always set at the critical value: 1/2. Starting the systems in an ordered state at $T = 0.6$ (a temperature well below the expected $T_c \simeq 1.41$), we increase T in steps of 0.1 until $T = 2.0$. Then the systems are cooled down, by the same steps, back to $T = 0.6$. At each temperature step, we evolve the systems by 20K MCS and used ten configurations from the last 1K MCS for measurements. Naturally, we will refer to these different segments having the same T's as the "heating" and "cooling" cycles.

To estimate the co-existing curve, we choose to measure directly the densities of the particle-rich clusters. Here, there is good reason to avoid using the "order parameter" of [16] and [17]. These authors introduced an "anisotropic magnetization":

$$m(\bar{\rho}) \equiv \frac{1}{\bar{\rho}(1-\bar{\rho})}\sqrt{< M_y^2 > - < M_x^2 >} \tag{4.1}$$

where

$$< M_x^2 > \equiv L_y^{-1}\left(\sum_y \left[L_x^{-1}\sum_x s(x,y)\right]^2\right)$$

and

$$< M_y^2 > \equiv L_x^{-1}\left(\sum_x \left[L_y^{-1}\sum_y s(x,y)\right]^2\right).$$

Since this is a non-analytic function, having little in common with the magnetization or a structure factor, the only rationales for such an unusual definition are the following. It is known that ordering occurs in strips along E, i.e., y, and $m(\bar{\rho})$ is normalized to unity for a completely ordered state, regardless of $\bar{\rho}$. Apart from known deficiencies of (4.1) for driven systems with PBC [26], completely ordered states with SPBC are *not* aligned with y, even in equilibrium. Also, we expect different types of ordering, into single strips aligned with the skewed axes as well as multiple strips aligned "vertically". Therefore, we decided to measure the densities directly. For that, we must find a working definition of, say, the particle-rich region.

One of the most widely applicable methods in statistical physics is the cluster algorithm [32]. A cluster is defined as the set of particles joined by nearest

neighbor bonds. In our case, we must be careful that SPBC is respected in identifying neighbors. Associated with a cluster, we employ two quantities: its mass (M_{clus}) and size (V_{clus}). The former is simply the total number of particles in the cluster. The latter, a measure of its volume (area in our $d = 2$ case), is defined as the number of sites within the cluster. To arrive at a well-defined notion of what the "boundary" of a cluster is, we build on the standard algorithms for finding a cluster. Specifically, for all sites *complementary* to the cluster in question, we set the occupation number to zero. These vacant sites will typically belong to a single giant cluster or a number of much smaller clusters (droplets of holes inside the particle cluster). Running the cluster algorithm for these sites will easily find the giant *hole-cluster*. The size of our original particle-cluster, V_{clus}, is then defined to be *the complement* of this giant hole-cluster. From its mass and volume, we define the density of a cluster:

$$\rho_{clus} = \frac{M_{clus}}{V_{clus}} \quad .$$

Needless to say, "microscopic" clusters with $M_{clus} \leq 6$ will have unit density and small ones will have densities close to 1, generally. As a result, it is interesting to examine distributions in the ρ_{clus}-V_{clus} plane. For random configurations, typical cluster sizes (V_{clus}) would be a few sites. For completely ordered configurations, the cluster mass would be exactly $\bar{\rho}LM$. At criticality, we expect a wide distribution in both cluster sizes and densities. Between $T = 0$ and criticality, there would be, ideally, a single (particle) cluster with $V_{clus} \sim V/2$ (i.e., 1296 in all our samples), so that its density will serve as the measure of co-existence. In practice, especially for systems with large aspect ratios, there are two or more smaller clusters which are of comparable density. Thus, we will include clusters greater than a third of the maximal size, i.e.,

$$V_{clus} \geq V/6 \tag{4.2}$$

in the statistics for computing the average $\overline{\rho_{clus}}$. Since we chose to focus on particle-clusters, $\overline{\rho_{clus}}$ should be greater than $1/2$. Given the particle-hole symmetry, we can improve statistics by also considering the hole-clusters under (4.2). The densities of hole-clusters (ρ_{hole}) are then averaged with $1 - \overline{\rho_{clus}}$. In Table 4.2 below, we will quote values of this final average, denoted by ρ for simplicity.

Finally, we point out an obvious advantage of the cluster method over pseudo-magnetizations like (4.1). With SPBC, it is expected that the ordered state may consist of a single strip of width $L/2$ but tilted from the vertical *or* a strip of width $L/2n$ wound around the torus n times, tilted or vertical. In all these cases, the cluster algorithm will find the connected domain and our method will find

its density. Of course, this method will be plagued by the presence of diffuse interfaces, which result from the drive being an extremely efficient mechanism for "evaporating" particles from a cluster. However, the only solution of the diffuse interface problem is to simulate very large lattices for very long times. Given the present computational limitations, our method is expected to provide a better picture of the co-existence curve than measuring quantities like (4.1).

4.2. Typical configurations in a "heating-cooling" cycle

In a series of figures, we show the typical configurations from a run. Each will consist of six figures, three from the "heating" phase of the cycle and three from the "cooling" phase. Though all runs range from $T = 0.6$ to 2.0 and back, we only show configurations from $T = 0.8, 1.0$, and slightly below criticality. These will give a good basis for discussing of the most interesting features.

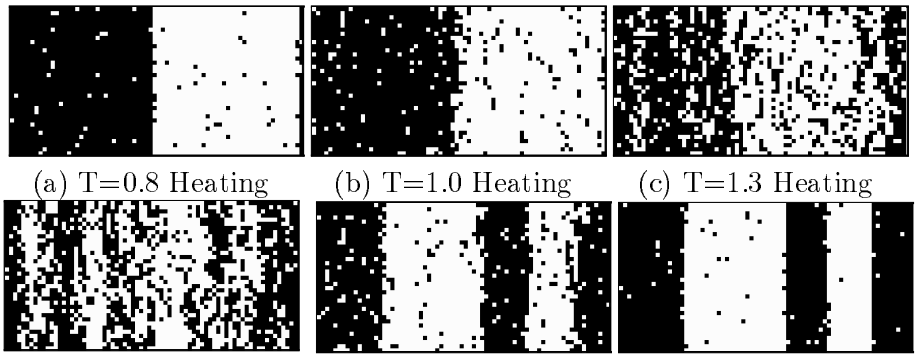

(a) T=0.8 Heating (b) T=1.0 Heating (c) T=1.3 Heating

(d) T=1.3 Cooling (e) T=1.0 Cooling (f) T=0.8 Cooling

Figure 4.1 Typical configurations for $H = 0$.

Figures 4.1a-f show configurations for a system with PBC ($H = 0$). As indicated, they come from different phases of the cycle. Since the initial state is a completely ordered state, it is not surprising that there is only a single cluster, with $V_{clus} \sim V/2 = 1296$, during the "heating" phase. On the other hand, as we see from Figs. 4.1e and 4.1f, the system has quenched into multistrip configurations, with two *disconnected* clusters. Of course, these states are metastable and will, after quite a long time in systems of these sizes, evolve into single cluster states. Instead of waiting for them to merge, we will see that the densities of the two clusters are comparable to the single clusters in Figs. 4.1a and 4.1b. Therefore, we have devised a rule for counting clusters which does not satisfy

$V_{clus} \sim V/2$. In particular, only the larger of the two clusters ($V_{clus} \sim 1000$) in these figures was used in computing $\overline{\rho_{clus}}$. More details will be presented in the next section.

Imposing SPBC has dramatic effects on the system, as the next four sets of figures show. Unlike systems with PBC, the refection symmetry, $R_x : x \to -x$, is lost. This can be traced, of course, to the lack of particle-hole symmetry in a driven system, but a combined symmetry, CR, remains [3]. Under CR, both $s \to -s$ and $y \to -y$ must be performed. With PBC, the transverse direction, x, is unaffected by the drive so that the system is invariant under R_x. Now, typical configurations consisting of particle-rich (or poor) regions tend to be uniform in y, in vertically aligned strips. Therefore, any significant inhomogeneities (in x) are R_x invariant. Obviously, SPBC mixes x and y, so that invariance under R_x is lost. Strips may not be aligned vertically and inhomogeneities in x are not necessarily invariant under R_x. A consequence is that particle-rich regions tend to be mirror images of particle poor ones. Therefore, it is prudent to use a convention which distinguishes these. In the rest of this thesis, we will reserved the word "*strip*" for *particle-rich* clusters only.

With this convention, we turn to the typical configurations. From the precursors observed in the disordered state, we may divide these into two categories: the low shift cases ($H = 3, 4$) and the high shift ones ($H = 9, 18$). Figures 4.2 and 4.3 show typical configurations in systems with low shifts.

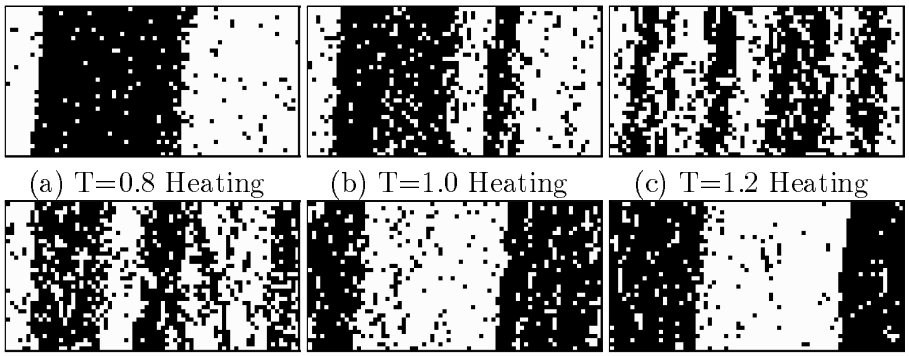

(a) T=0.8 Heating (b) T=1.0 Heating (c) T=1.2 Heating

(d) T=1.2 Cooling (e) T=1.0 Cooling (f) T=0.8 Cooling

Figure 4.2 Typical configurations for $H = 3$.

In Figures 4.2a-f we first note that all the strips tend to be "tilted" in accordance to the SPBC. Next, we point out, in both of the $T = 0.8$ systems, that the right edge of a strip is much more diffuse, since the drive tends to tear particle out

of the cluster. Thus, we may think of this as the "evaporating edge", acting as a particle source for the hole-rich region. Conversely, E tends to drive particles into the strip on the left edge. Acting as a sink for particles, we call it the "absorbing edge". The combined effect on the strip is a non-trivial drift in x. Our observation is that strips drift to the *right*, with narrow strips moving faster. It is unclear why the drifts are of this sign. Unlike a similar phenomenon in a driven *two species* system [19], there is no theoretical basis that the drift must be of one sign. As the temperature increases (Fig. 4.2b), we see that the drive has evaporated so many particles from the large cluster that a narrow strip has recondensed to its right ("down stream"). Since narrow strips drift faster, they tend to move around and merge with the large strip subsequently. Fig. 4.2e shows a configuration at the same temperature, but no "break away" strips. This phenomenon is observed at temperatures as low as $T = 0.9$! Complicating the situation, narrow strips are also more susceptible to complete evaporation. In this sense alone, systems with SPBC pose a serious challenge to an unequivocal definition of "non-equilibrium steady state". By $T = 1.2$ (Figs. 4.2c,d), we see that even large fluctuations are present, with a multiplicity of narrow strips which occasionally merge to form large clusters of low density. Comparing the cluster in Fig. 4.2a to that in Fig. 4.2c, we may use the adjectives "compact" and "rarified". As we will see below, this violent dynamics is reflected in the large variations of both the cluster sizes and densities.

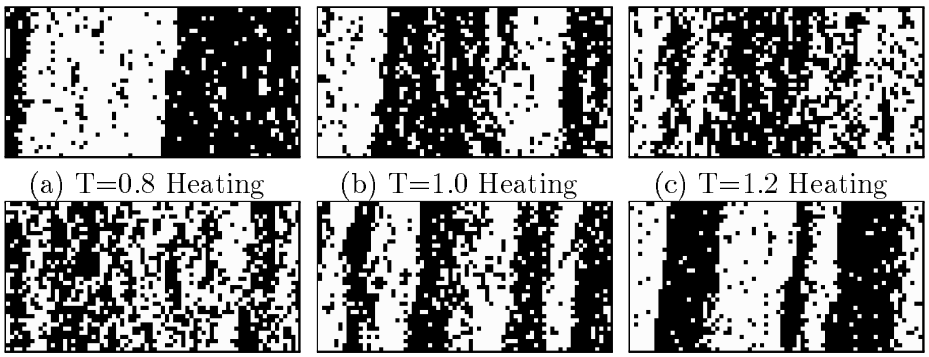

Figure 4.3 Typical configurations for $H = 4$.

Figures 4.3a-f show that the $H = 4$ system is similar to the one with shift 3. Of course, the strips are tilted in accordance with a shift of four. More importantly, "break away" strips are already present at $T = 0.8$, while the $T =$

1.0 configurations here (Figs. 4.3b,e) resemble the $T = 1.2$ configurations in $H = 3$. Fluctuations are more violent, indicating the destruction of a simple phase separated state with increasing shift. Indeed, we find that the behavior of the $H = 6$ system is so far beyond the standard descriptions that we defer the discussions to chapter 6. Surprisingly, when the shifts are high enough, the system becomes more "well- behaved". Thus, we skip to the $H = 9, 18$ cases next.

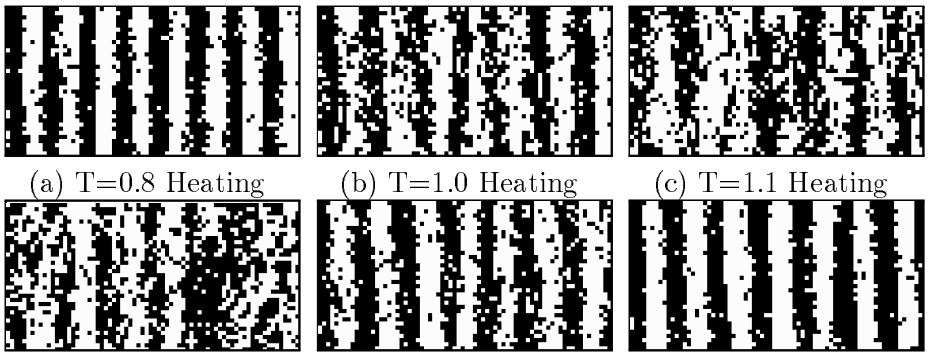

(a) T=0.8 Heating (b) T=1.0 Heating (c) T=1.1 Heating

(d) T=1.1 Cooling (e) T=1.0 Cooling (f) T=0.8 Cooling

Figure 4.4 Typical configurations for $H = 9$.

From Figures 4.4a-f, it is clear that the ordered states of a $H = 9$ system are dramatically different from the low shift ones. Even Starting with a solid single tilted strip, the system quickly evolves, even at very low temperatures, to "multi-strip" states like those in Figs. 4.3a,f. Unlike the multistrip configurations in the $H = 0$ case, these regions are *connected* via the SPBC. It is actually a single strip multiply wound around the torus, 8 times in this case. In particular, the cluster algorithm will find only a single large cluster. Due to topological constraints, there is a simple relationship between Ω, the multiplicity of the winding, and the alignment of the strip, for low and high shifts:

$$\tan\theta = \frac{H - L/\Omega}{M} \tag{4.3}$$

where θ is the angle the strip makes with the y-axis. Parenthetically, note that, for the single strip configuration, the effective Ω is not unity, but infinity. In general, L is not divisible by H so that θ cannot assume the value 0. For example, θ can be negative for $H = 6$, $\Omega = 10$ as shown in Figure D.1 in Appendix D. In previous

studies [15], multiple strips not aligned vertically are seen most frequently. Given that our systems are half filled, the widths of the strips must be, on the average,

$$w = \frac{L}{2\Omega}. \tag{4.4}$$

Not surprisingly, a system prefers to be in states with small θ, in general. However, from the only other study on driven lattice gases with SPBC [15], it does not appear to be an absolute criterion. Obviously, more extensive investigations are needed before this issue can be resolved.

Returning to our case, $\theta = 0$ is allowed and we have vertically aligned strips. Thus, unlike in the low shift cases, there is no drift. In this sense, the similarity to the $H = 0$ system is greater than the low shifts cases. In more detail, comparing Figs 4.4a and 4.1a, we see that the cluster densities are also similar, even up to $T = 1.0$. Above that, the two systems seem to diverge. Since the strips here are very narrow, it is easier for them to "evaporate", with the result that large, rarified clusters are often found, e.g., in Figs. 4.4c,d. By contrast, the phenomenon is absent in the $H = 0$ system until $T \gtrsim 1.3$.

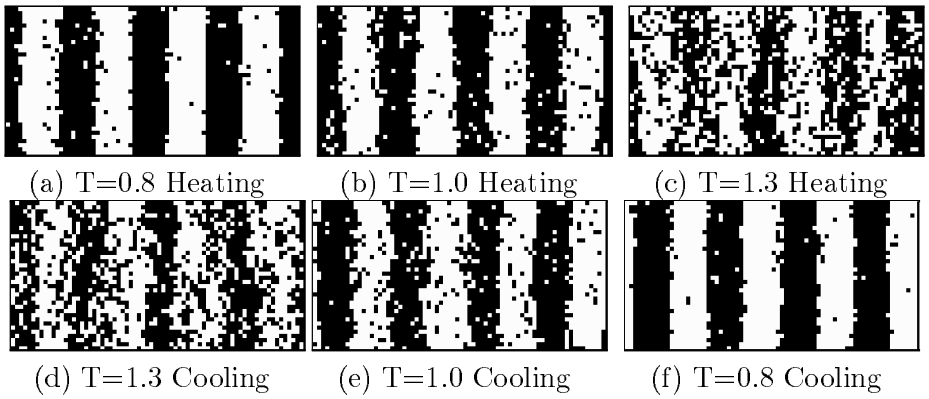

(a) T=0.8 Heating (b) T=1.0 Heating (c) T=1.3 Heating

(d) T=1.3 Cooling (e) T=1.0 Cooling (f) T=0.8 Cooling

Figure 4.5 Typical configurations for $H = 18$.

The $H = 18$ system behaves in a fashion very similar to the $H = 9$ case, as shown in Figures 4.4a-f. Yet, the H=18 system maintains order even at $T = 1.3$, just like the H=0 case! At the lower temperatures, vertical "multistrips" are predominant, with $\Omega = 4$. The widths are correspondingly twice as large as in the $H = 9$ case, so that the cluster densities are somewhat lower. Again, these are comparable to the $H = 0$ system. Due to the strips being wider than those in the $H = 9$ case, "evaporation" and large fluctuations do not set in until slightly higher temperatures.

4.3. Cluster sizes, cluster densities, and the co-existence curve

From the typical configurations, we may conclude that the rate of the temperatures changes (0.1/20K MCS) is probably too fast for some cases. Ideally, we may use faster rates far from criticality, but should use slower ones for $T \sim T_c$. Nevertheless, we believe that our data can give us a rough estimate of the coexistence curves and display important differences between systems with different shifts. Using the methods described in the first section of this chapter, we summarize our finding in the following tables.

Though cluster sizes will not be directly used for constructing the co-existence curve, we provide their statistics in Table 4.1 for completeness. Absent entries for low temperatures are not significant, since the system is so ordered at T's higher than these that it is unnecessary to quote specifics. On the other hand, absent entries under $H = 9$ indicate that no cluster satisfying (4.2) is present. These missing entries are a strong indication of the critical temperature for these systems.

Table 4.1 Cluster size statistics: average±standard deviation

T\ H	H=0		H=3		H=4	
	heating	cooling	heating	cooling	heating	cooling
T=0.6	-	-	1294±11	1294±7	1294±10	1292±26
T=0.7	-	-	1294±11	1293±14	789±206	690±178
T=0.8	1294±8	915±18	1293±19	1296±26	1288±23	526±60
T=0.9	1293±10	926±30	1145±70	797±189	730±120	1010±66
T=1.0	1292±18	799±166	1160±106	1081±299	769±182	501±50
T=1.1	1299±22	808±169	667±114	636±154	779±276	583±117
T=1.2	1290±26	779±230	682±192	540±80	970±237	728±153
T=1.3	1279±56	885±274	616±130	697±190	1014±305	607±175

T\H	H=9		H=18	
	heating	cooling	heating	cooling
T=0.6	1294±4	1294±5	-	-
T=0.7	1288±1	1292±6	-	-
T=0.8	1291±5	1290±8	1293±11	1293±5
T=0.9	1276±3	1287±12	1292±12	1292±12
T=1.0	1294±3	1280±30	1288±16	1288±11
T=1.1	-	-	1281±24	1284±21
T=1.2	-	-	1268±26	1274±41
T=1.3	-	-	1204±176	1005±212

With reference to the typical configurations shown above, we see that, typically, a single large cluster prevails to higher temperatures during the heating cycle. This reflects the fact that, on cooling, the system frequently condensed first into two or more disconnected strips. Using the cut-off defined in (4.2), typically the largest of these will be included in the statistics. It is easy to appreciate that there is little variation in the sizes cluster with $V_{clus} \sim V/2 = 1296$, while large variations are common for smaller ones. With these cautionary remarks, we conclude that $T_c > 1.3$ for the $H = 0, 18$ systems, but that, for low shifts and $H = 9$, criticality sets in at lower temperatures.

Next we turn to the main subject at hand: densities of cluster below criticality, shown in Table 4.2a,b. Recall that ρ comprises of the density of hole clusters as well as $1 - \overline{\rho_{clus}}$. Further, we normalized it to 36, the number of sites in a column. So, an entry like $\rho = 3.9 \pm 0.9$ ($T = 1.0; H = 0$) means a density of "three to five particles per column". We use this normalization in anticipation of a discussion of the distribution of column densities in the next chapter.

Though the cluster sizes may vary by as much as a factor of three over heating and cooling cycles, their densities are much more consistent. However, we emphasize that, typically, smaller clusters are denser. Therefore, we chose a criterion: (4.2), excluding clusters smaller than $V/6$. Not surprisingly, there is some correlation between the variations in cluster size and those of the cluster density. Nevertheless, as we examine Table 4.2 we see that, on the average, the densities between heating and cooling cycles lie within the standard deviations quoted.

Table 4.2a Cluster density statistics (average±standard deviation) for systems with PBC and low shifts

$T\backslash H$	$H = 0$			$H = 3$		
	heating	*cooling*	ρ	*heating*	*cooling*	ρ
$T = 0.6$	–	–	–	3.5 ± 0.7	4.0 ± 0.8	3.8 ± 0.8
$T = 0.7$	–	–	–	3.8 ± 1.2	5.0 ± 1.7	4.4 ± 1.6
$T = 0.8$	1.5 ± 0.3	1.4 ± 0.3	1.5 ± 0.4	6.4 ± 0.5	4.1 ± 1.0	5.0 ± 1.4
$T = 0.9$	2.8 ± 0.4	2.8 ± 0.3	2.8 ± 0.4	8.7 ± 3.2	7.2 ± 2.0	8.0 ± 2.8
$T = 1.0$	3.9 ± 0.5	3.9 ± 0.9	3.9 ± 0.9	9.5 ± 1.5	8.3 ± 2.1	9.0 ± 1.9
$T = 1.1$	7.9 ± 0.5	6.0 ± 1.0	6.7 ± 1.2	14.6 ± 5.3	13.2 ± 3.6	13.9 ± 4.6
$T = 1.2$	9.1 ± 0.6	8.8 ± 1.3	8.9 ± 1.1	16.2 ± 3.4	15.1 ± 4.8	15.8 ± 4.2
$T = 1.3$	13.4 ± 1.0	16.8 ± 4.2	15.2 ± 3.2	–	–	–

$T \backslash H$	$H = 4$		
	heating	*cooling*	ρ
$T = 0.6$	3.5 ± 0.7	4.1 ± 0.8	3.8 ± 0.8
$T = 0.7$	3.8 ± 1.2	5.0 ± 1.7	4.4 ± 1.6
$T = 0.8$	6.4 ± 0.6	4.1 ± 1.0	5.0 ± 1.4
$T = 0.9$	8.7 ± 3.2	7.2 ± 2.0	8.0 ± 2.8
$T = 1.0$	9.5 ± 1.5	8.3 ± 2.1	9.0 ± 1.9
$T = 1.1$	14.6 ± 5.4	13.2 ± 3.6	14.0 ± 4.6
$T = 1.2$	–	–	–
$T = 1.3$	–	–	–

Table 4.2b Cluster density statistics (average±standard deviation) for systems with high shifts

$T \backslash H$	$H = 9$			$H = 18$		
	heating	*cooling*	ρ	*heating*	*cooling*	ρ
$T = 0.8$	1.0 ± 0.04	1.5 ± 0.3	1.3 ± 0.4	1.4 ± 0.5	1.2 ± 0.2	1.3 ± 0.4
$T = 0.9$	1.7 ± 0.4	2.3 ± 0.4	2.2 ± 0.5	2.3 ± 0.5	2.2 ± 0.5	2.2 ± 0.5
$T = 1.0$	3.6 ± 0.4	3.2 ± 0.7	3.5 ± 1.0	3.6 ± 0.6	3.6 ± 0.4	3.6 ± 0.5
$T = 1.1$	–	–	–	5.3 ± 1.0	5.5 ± 0.8	5.4 ± 0.8
$T = 1.2$	–	–	–	7.5 ± 0.7	8.0 ± 1.3	7.9 ± 1.2
$T = 1.3$	–	–	–	10.1 ± 1.1	11.4 ± 1.8	10.8 ± 1.6

Finally, using the densities in Table 4.2, we plot the curves for phase coexistence in Figures 4.6.

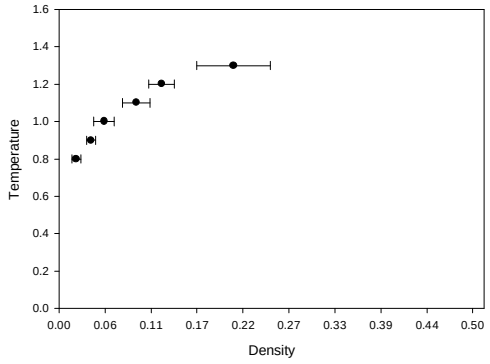

(a) H=0

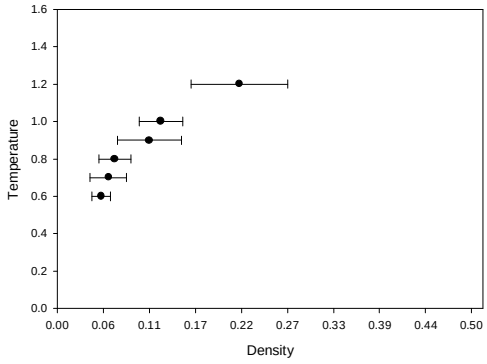

(b) H=3

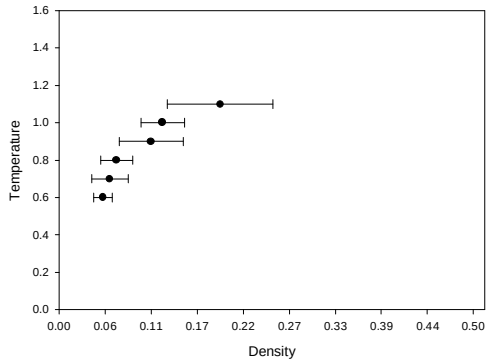

(c) H=4

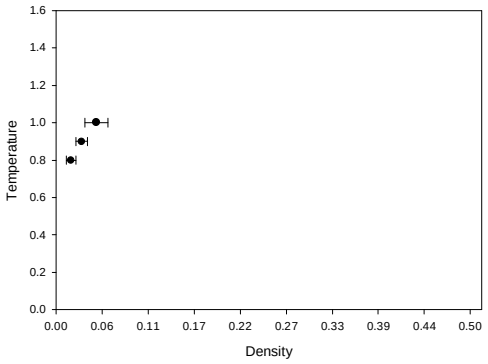

(d) H=9

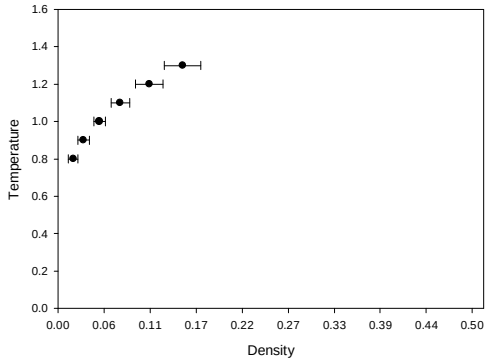

(e) H=18

Figure 4.6 Coexistence curves: temperature vs. cluster densities

The generally trend is clear: SPBC has a dramatic effect on phase co-existence. For low shifts, the co-existence curve "shrinks". In fact, it seems that there is no simple concept of phase-coexistence for $H = 6$, as we will see in Chapter 6. However, for larger shifts, the system accommodates the SPBC by ordering into a new type of state, i.e., single strip with multiple windings. In fact, it would be reasonable to conclude that the ordered states of $H = 9$ and 18 are *distinct*. As a previous study [15] hinted, there are transitions between states with distinct Ω which resemble the "break-up" we observe for the $H = 6$ system. Since the shifts we have used are commensurate with the system size, so that the strips can be vertically aligned, we have explored only the "simple" cases. Clearly, it would be interesting to carry out a systematic study for all other shifts and on large lattices. If our picture is correct, there would be, *for each* Ω, a family of "nested" co-existence curves. It is remarkable how the simple microscopic dynamics of a driven lattice gas with SPBC can lead to such rich and complex phenomena.

5. Order-disorder transitions: phase diagram in the $\bar{\rho}$-T plane

An alternative method to measure the co-existence curve is to use systems with a range of *overall densities* $\overline{\rho} \neq 1/2$ as well as various temperatures T. A phase diagram in the T-$\overline{\rho}$ plane can be constructed by observing whether the system is homogeneous and disordered or inhomogeneous and phase segregated. Of course, for systems in equilibrium and in the thermodynamic limit, the boundary between the disordered and ordered phases should be precisely the co-existence curve: $\rho_{\pm}(T)$, found by the method in Chapter 4. For finite systems, differences are expected. While careful extrapolations will be necessary to extract the unique co-existence curve, here we will be content with *consistency* of results obtained with these two methods.

In this approach, clearly we must rely on some definition of ordering. In addition to measuring cluster sizes and densities, we decided on three other "order parameters." Each has advantages and deficiencies. Thus, the first section of this chapter will be devoted to a discussion of the various order parameters. In the second section, we show the data for each of these, tracking them as we vary T (with $\overline{\rho}$ held constant) or $\overline{\rho}$ (with fixed T), depending the region of the phase diagram explored. The choices are dictated by the expected slop of the co-existence curve. All these plots yield a consistent picture for $\rho(T)$, albeit a rough one, for each of the five shifts $H = \{0, 3, 4, 9, 18\}$. Again, the $H = 6$ system will be treated separately in Chapter 6. We construct $m(T)$ for systems subjected to SPBC with six different shifts, H.

5.1. Order Parameters

Since the system displays relatively complex behavior, exploring it with a variety of measures will provide crucial cross checks of the estimates of the co-existence curves and give us confidence in our conclusions. In particular, we expect ordering into strips not only along the field ("vertical") and along the skewed axes ("tilted") imposed by the shifted periodic boundary conditions, but also into strips of multiple winding of a range of other angles (4.3). In chapter 3 we de-

fined "skewed" structure factors $\tilde{S}_h$ in an attempt to measure correlations above T_c. Here, they will serve as an order parameter for states with tilted strips, in much the same way that ordinary structure factors are standard measures for vertical strips. For systems with $\bar{\rho} \neq 1/2$, a completely ordered state will carry sizable intensities in so many components that it may be difficult to discern the signal of ordering by examining the structure factors. Thus, we consider densities of individual columns. Similarly, two types of columns densities are defined: *tilted* and *vertical*. Histograms and fluctuations of these densities clearly carry the message of ordering. Finally, we also determine order by measuring the properties of the clusters and the total "internal energy".

5.1.1. Structure Factors

In Chapter 3, we have introduced both the standard structure factors $S(\mathbf{k})$ and the skewed version $\tilde{S}_H(\bar{\mathbf{k}})$. Since our systems obey conserved dynamics, $S(\mathbf{0})$ is a constant, depending on the overall density $\overline{\rho}$ (or the total "magnetization"). With our normalization, the total intensity, $\sum_{\mathbf{k}} S(\mathbf{k}) = \sum \tilde{S}_H$, sums to $V = 2592$. For a random configuration, each S or $\tilde{S}$ would be 1, which is the typical value for the entries in Tables 3.1, 3.4, and 3.5. For an ordered state, intensities appropriate for that state will be $O(V)$, as we illustrate in Appendix C. In a finite system, there the crossover from $O(1)$ behavior to $O(V)$ is necessarily smooth, so that the transition point can only be estimated. With data from a range of sizes, simple extrapolation methods or sophisticated finite size scaling analyses can be used to arrive at more accurate determination of the transition point. In this first study of phase transitions in systems with SPBC, we have confined to one size only, so that our results are expected to be reliable to 10%. Finally, as in Chapter 3, we exploited the averages $< P_0 >$, $< \tilde{P} >$, $< \tilde{P}_0 >$, and $< \tilde{P} >$, as an overall measure of correlations, regardless of the variety of states in which clustering favors. For ordering, this "trick" is equally important. Thus, we will be quoting results for these quantities as well.

5.1.2. Column densities and fluctuations

In our simulations, temperature settings will be lowered as well as raised. As a result, configurations frequently spend extended periods of time in metastable states with multiple strips of varying widths, even if the final steady state comprises of only a single strip. Though these states should not, strictly, be counted in the final ensemble average, the densities in the strips appear to be approximately the same as that in the steady state. With limited time resources and with our focus only on the transition to phase co-existence, we decided to keep

these data and devised a method of taking only the relevant densities into account. Since they are of varying widths, structure factors will not be a good guide. Instead, observing that the strips typically span the vertical dimension of the sample, we turn to measuring *column densities*. In other words, column densities are designed according to the strong anisotropy of the system, i.e., most condensed regions are aligned along, more or less, the external field.

The column densities are a measure of the occupation in a lattice column. The idea is that, for a disordered state, these densities will be the overall density $\bar{\rho}$, on the average. However, for a completely ordered state, they would be typically 1 or 0, depending on whether the column lies within a strip or not. Since we deal only with systems of a single size so that density and occupation number differ only by $M = 36$, we find it convenient to use the latter and merely count the number of particles in a column. Thus, all the values of our column "densities" are normalized to 36.

One complication is that, since we are expecting different types of alignment, we must define different types of column densities. For vertical alignment, the most sensitive measure is

$$\rho_0(i) = \sum_{j=1}^{36} n(i,j). \tag{5.1}$$

For systems with low shifts ($H < 6$), the strips are typically tilted and even totally ordered states will show a distribution in $\rho_0(i)$. Thus, we are led to introduce a "skewed column" density which is tuned to the particular shift in question:

$$\rho_h(i) = \sum_{j=1}^{36} \eta(i + [(j-1)H/36]\ ,\ j) \tag{5.2}$$

where, again, $[\cdot]$ stands for the integer part of $\cdot$. For convenience, we will refer to the column densities collectively as ρ_{col}. For a system with a specific H, only ρ_0 and ρ_H are measured and histograms are constructed. Since ordering in systems with large shifts ($H = 9, 18$) tends to be "vertical", the former will turn out to be adequate. In a systematic study, we would measure ρ_h with $h \neq H$ in order to be sensitive to multiple windings leading to strips aligned non-vertically.

As an illustration of these methods, we provide two examples in Figures 5.1a,b. Both can be completely ordered states in a $H = 18$ system, with multiple windings of $\Omega = 4, 6$ respectively. The associated histograms are shown in Figures 5.2a,b. In the first case, we see that the distribution for ρ_0 is *bi-modal*, properly identifying the state as being phase separated. Yet, the distribution for ρ_{18} is single peaked, which is the characteristic of a disordered state. In the second example, the distribution for ρ_0 is almost flat, whereas the distribution for ρ_6 shows the clear

signal for perfect order. Below, we will see similar distinctions in the histograms of the actual runs, so that we may infer not only whether a transition took place but also which state the ordering is favoring. Finally, we re-emphasize that, to compile the histograms for the simulations, we used ten configurations in the latter part of each of the temperature steps.

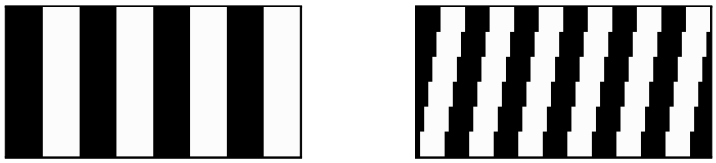

(a) (b)

Figure 5.1 Ordered states for a $H = 18$ system with (a) $\Omega = 4$ and (b) $\Omega = 6$

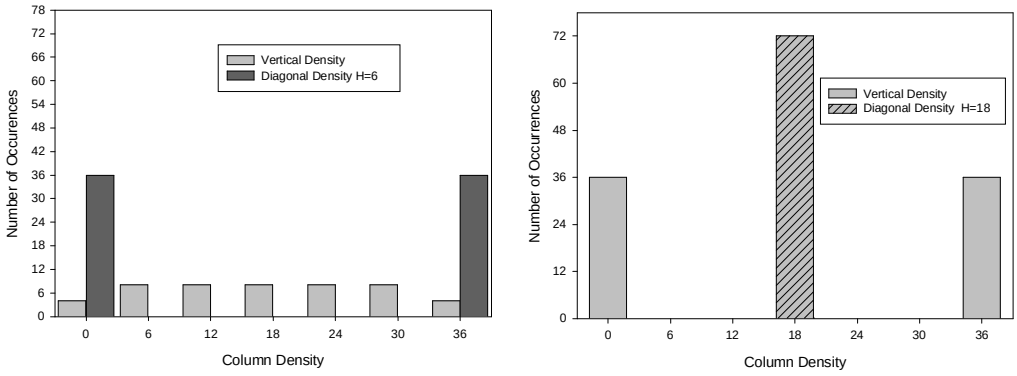

Figure 5.2 Histograms associated with Figures 5.1a,b respectively

From a histogram, more compact measures can be extracted, e.g., its average and its standard deviation. The former is fixed, due to the conserved dynamics, at $\bar{\rho}M$. The latter, or the width, carries information about ordering. Far into a disordered state, the distributions are well approximated by Gaussians about the average, so that the widths,

$$\Delta\rho_h \equiv \sqrt{< \rho_h^2 > - (\bar{\rho}M)^2} \tag{5.3}$$

with $h = 0,3$, etc., should be "small": $O(\sqrt{M})$ and related to a generalized susceptibility. On the other hand, deep into an ordered state, the distributions

should be double peaked, at the values corresponding to the densities of the co-existing phases. Therefore, (5.3) will become "large", i.e., $O(M)$. As we will see, for the standard system ($\bar{\rho} = 1/2, H = 0$), $\Delta\rho_{\mathbf{0}}$ varies smoothly, like the structure factor S, as T is raised and lowered through T_c. However, for $\bar{\rho} = 1/9$ ($H = 0$), it jumps discontinuously, typical of other features at the co-existence curve away from the critical point.

The single-peak to bi-modal transition in the distribution is a familiar phenomenon associated with symmetry breaking. For systems with *Ising symmetry*, a standard way to "avoid" the bi-modal distribution is to construct histograms for the square of the magnetization. Another way is simply to take the magnitude of the magnetization. In the density language, this procedure consists of nothing but "folding" the histograms about the mid-point $M/2$ (18 in our case). Below, we display only one set of such "folded" histograms (Figure 5.11). Note that the abscissa is the absolute value of the "magnetization" and so, normalized to unity. Of course, the disadvantage of this approach is that the averages are less accessible analytically, especially in the case of $\rho_{h\neq\mathbf{0}}$. Nevertheless, we find this description useful, since the widths of these "folded distributions"

$$\Delta(FD) \equiv \sqrt{\left\langle \left(\frac{\rho_h}{18} - 1\right)^2 \right\rangle - \left\langle \left|\frac{\rho_h}{18} - 1\right|^2 \right\rangle} \tag{5.4}$$

should be "small", both above and below criticality. Indeed, in both regimes, this quantity is intimately related to the "susceptibility". In the neighborhood of the transition, the widths serve as good indicators of large fluctuations, so that peaks in the plot of $\Delta(FD)$ vs T can serve to locate the transition temperature.

When presenting the picture for "folded histograms", we have glossed over an important feature which, unfortunately, muddies an otherwise clear picture. Even for these histograms, the distributions are bi-modal below criticality! There is a small peak near the origin, which can be traced to the presence of the interfaces. Due to thermal fluctuations, these are of non-zero width, so that the densities interpolate smoothly through 1/2, between $\rho_{\pm}$, the densities of the co-existing domains. Since $\rho = 1/2$ is mapped into the origin in a folded histogram, there is a small peak here. It is possible to systematically extract this contribution, by using systems with different L's. However, that is beyond the scope of this thesis. Here, we arbitrarily remove these part of the histogram by imposing a cut after a *coarse-grain* procedure.

The method of coarse graining [CG], inspired by the renormalization group [33], involves averaging the densities of every three column densities. For every

set of three, each CG density (ρ_h^{CG}) assumes the average value:

$$\rho_h^{CG}(i) = \rho_h^{CG}(i+1) = \rho_h^{CG}(i+2) = \frac{1}{3}\sum_{k=0}^{2} \rho_h(i+k). \tag{5.5}$$

This procedure is designed to sharpen the peak associated with the ordered domain, since it maps a systems to a lower effective temperature. The peak associated with interfaces is also more exposed, leading to a somewhat less arbitrary scheme for its removal. Thus, all figures for $\Delta(FD)$ are compiled for histograms which have been folded *and* coarse grained.

5.1.3. Cluster sizes and densities

This method is identical to that used in Chapter 4. For each cluster, we focus on two of its characteristics: density (ρ_{clus}) and size (V_{clus}). Most clusters in a disordered phase at high temperatures will be small (and therefore dense). On the other hand, in a completely ordered state, there would be only one giant and cluster of unit density, while a wide distribution of densities and sizes is expected in the neighborhood of a transition. Thus, histograms in ρ_{clus}-V_{clus} should serve as a good indication of the transition. In the plots shown below, the distributions are actually constructed from the *total mass* of the clusters in each bin, instead of the total number of such clusters. The reason for this is clear: a histogram of a completely ordered state would be practically invisible compared to that for a disordered state. The other advantage of using the mass is normalization: the integral would be just $\bar{\rho}LM$. Finally, a composite plot of the data from all T (with $\bar{\rho} = 1/2$), in the ρ_{clus}-T plane, is quite revealing. As we will see, there exists a sharp boundary, which will be identified with the co-existence curve itself.

5.1.4. Internal energy

The internal energy is simply the energy associated with a configuration according to (1.2). For a system with fixed total number of particles, it is just as convenient to use the spin language so that, apart from an overall constant, the internal energy is proportional to the number of "broken" bonds (nearest neighbor pairs of opposite spin). For simplicity, we will quote this number when we refer to the internal energy.

For the Ising model in equilibrium, this quantity offers yet another standard tool for identifying phase transitions, since its derivative with respect to T is the specific heat. We believe that it can also serve as an indicator of non-equilibrium transitions. In particular, for a completely ordered state it is just $2(36+H)$, for

any $\bar{\rho}$. Needless to say, multistrip states have higher energy, due to the extended interface. For random configurations, the *average* would be $2\bar{\rho}\,(1-\bar{\rho})\,LM$. With a variety of finite sizes and aspect ratios, the average internal energy U can be used to detect the number of strip as well. We used it in our investigation of the 2×3 system in Chapter 2. Finally, in a physical system, U is of course an be easily measured experimentally.

5.1.5. Co-existence curves

With these different means of measuring whether a system is ordered or disordered, we turn to the simulation results themselves. Since there is a considerable amount of data, we will only discuss in detail how these methods are applied to two cases, namely, varying T on systems with $\overline{\rho} = 36/72$ and $8/72$ subjected to PBC ($H = 0$). For the other shifts ($H = 3, 4, 9, 18$), as well as runs with varying $\bar{\rho}$ with fixed T, we only report the results in a series of figures. This chapter ends with our goal: a series of co-existence curves.

5.2. Two systems with PBC (H=0)

As a reminder, each constant density "run" starts with a system in a completely ordered state and allowed to evolve for 20K MCS with the temperature set low enough that the system should be phase separated. Then T is raised, in steps of 0.1, until well into the homogeneous phase. After that, it is lowered by the same set of steps till the original temperature is reached. This heating-cooling cycle allows us to observe hysteresis and provides us with bounds on transitions which are first order. At each step, the system is evolved for 20K MCS and then measurements made. Most data are presented as a pair of diagrams, half for the heating part and half for the cooling part of the run. For the $\overline{\rho}$=36/72 system, the temperature range is $[0.5, 2.0]$. Figure 5.3 shows some of the typical configurations used for the measurements.

(a) T=1.0 Heating (b) T=1.4 Heating (c) T=2.0

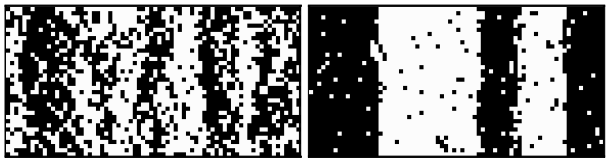

(d) T=1.4 Cooling (e) T=0.9 Cooling

Figure 5.3 Typical configurations for $\overline{\rho} = 36/72$, $H = 0$

For the $\bar{\rho} = 8/72$ system, the temperature range is $[0.5, 1.4]$. Figure 5.4 shows some of the typical configurations.

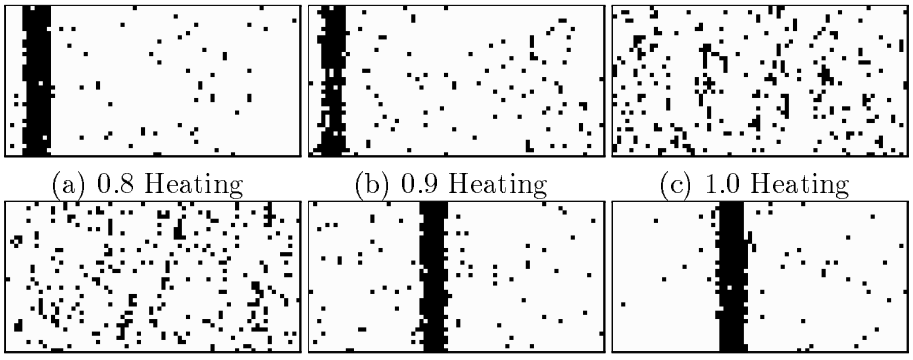

(a) 0.8 Heating (b) 0.9 Heating (c) 1.0 Heating

(d) T=0.9 Cooling (e) T=0.8 Cooling (f) T=0.7 Cooling

Figure 5.4 Configurations for $\bar{\rho} = 8/72$, $H = 0$

For measurements, we select ten configurations from the last thousand MCS in each 20K MCS set. Except for those near criticality, we hope that the system has more or less settled to the new temperature when the data are taken. However, it may be caught in some metastable state and, as pointed out above, some of our methods are designed to circumvent this difficulty. Clearly, with enough time and resources, we would be able to wait until the system to stabilize completely. To accomplish our goal, establishing co-existence curves at the 10% accuracy level, it is sufficient to use such coarse methods.

The first tool involves the *structure factors*. Since both of these systems are not shifted, it is unnecessary to consider skewed versions and only results for $S(\mathbf{k})$ are quote. In Figure 5.5, shows $S(n_x, 0)$ for $n_x \in [1, 9]$. At each n_x, there are five bars, one for each of the T's shown in Fig. 5.3. Meanwhile, the intensities for the high n_x's remain $O(1)$, typical of those for random configurations. For the low n_x's, we see clearly the signal of the transition in both directions. Note however,

the differences between the heating and cooling phases. In the heating phase, only a single strip is present, so that $S(1,0)$ dominates, as seen in the $T = 1.0$ bars. By contrast, on the cooling part of the cycle, other structure factors become large as well, notably $S(2,0)$ and $S(4,0)$. This behavior is, of course, associated with the phenomenon of phase separation into more than one strip, as in Fig. 5.3(e).

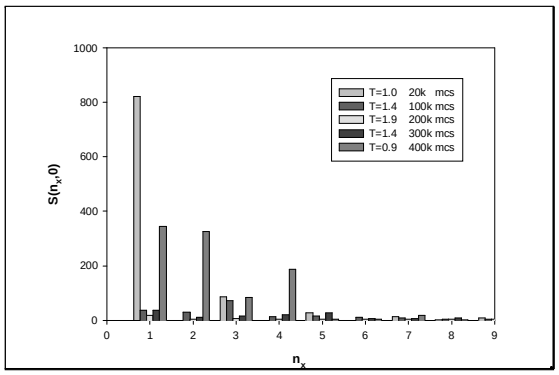

Figure 5.5 The first nine $S(n_x, 0)$ at T's corresponding to Fig. 5.3.

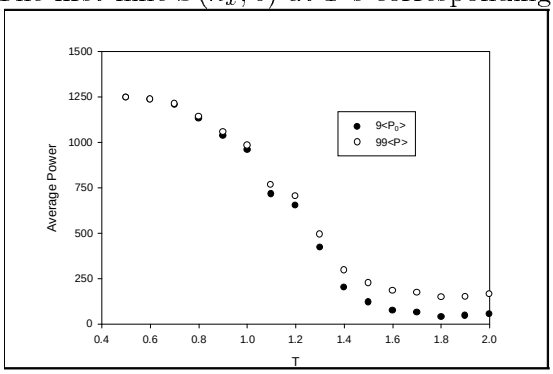

Figure 5.6 Sums of $S(n_x, 0)$ during the heating cycle ($\bar{\rho} = 36/72$, $H = 0$).

Since multistripped metastable states are unavoidable in the cooling cycle, it is reasonable to focus on the sum of the intensities, as opposed to focussing only on, say, $S(1,0)$. Thus, we plot, in Figure 5.6, the sum over the nine $S(n_x,0)$'s, as well as over all $S(n_x,0)$ for $n_x, n_y \in [1,9]$. We have expressed these as the averages $< P_0 >$ and $< P >$ introduced previously. For high temperatures, we see that the averages are approximately equal, with the sums differing by about a factor of 10.The merging of these two sums at low temperatures is just another perspective on the fact that the intensities at the low n_x's are dominant and that

the system displays only one vertical strip. The location for the transition is quite clear, at least at the level of accuracy expected in a finite system like ours.

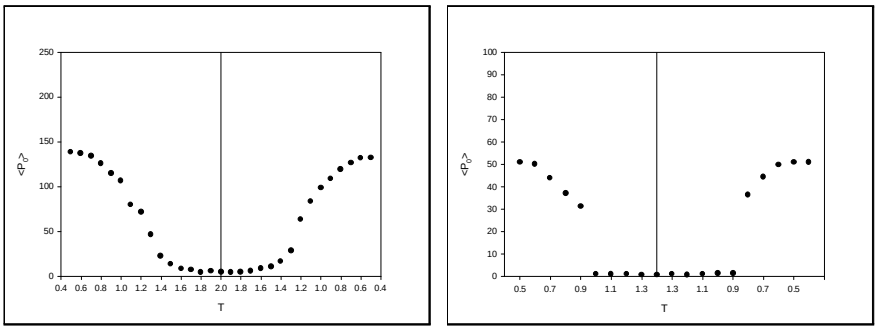

(a) $\bar{\rho}$=36/72 (b) $\bar{\rho}$=8/72

Figure 5.7 The average intensity $< P_0 >$ for the (a) $\overline{\rho} = 36/7$ and (b) 8/72 systems.

From Fig. 5.6, we see that it is adequate to use $< P_0 >$ alone for identifying the transition. Thus, we will plot only this quantity for all the other cases to be presented. In particular, Figures 5.7a,b show $< P_0 >$ for the $\overline{\rho} = 36/7$ and 8/72 systems, respectively. On the left (right) part of each figure, we display the dependence of this quantity on T, during the heating (cooling) phase of the run. Note that $< P_0 >$ for the cooling part in Fig. 5.7a is comparable to the heating part. Had we used $S(1,0)$, there would be a substantial difference. But, $< P_0 >$ consists of other intensities, such as $S(2,0)$ as well, so that it is sensitive to a system ordering into one or two vertical strips with large density. It is reassuring that, using this method, the location of the transition, $T \simeq 1.3$, does not differ much between the two parts of the cycle. For the $\bar{\rho} = 8/72$ system, the overall scale for $< P_0 >$ is less, as a completely ordered strip is only 25% the size of that in the $\overline{\overline{\rho}} = 36/72$ system. The most striking difference is clearly the discontinuity as the system disorders during the heating cycle, between $T = 0.9$ and $T = 1.0$. We also observe hysteresis, since the jump occurs between $T = 0.9$ and $T = 0.8$ as the system is cooled. Presumably, with slower sweeps, the gap can be narrowed. A reasonable estimate of the transition temperature would be $T = 0.9 \pm 0.1$. The uncertainty comes from the temperature step size and the hysteresis phenomenon.

Next, we turn to the behavior of *column densities*. As mentioned above, both the drive and the PBC favor vertical alignment, so that we may consider only the "density" in vertical columns: ρ_0. Recalling that this quantity is normalized to

36 for a filled column, we present histograms for ρ_0 in Figure 5.8, corresponding to the settings which resulted in the typical configurations in Fig. 5.3. The area under the histograms is 720, reflecting our choice of using ten configurations of 72 columns each. The distinction between an ordered, phase separated state and a disordered, homogeneous state is vividly displayed. One distribution is sharply bi-modal, concentrated at the ends of plot, while the other is resembles more a Gaussian. Large fluctuations near the transition are also evident in the two $T = 1.4$ plots (Figs. 5.8b,d). Finally, we point out the similarities between Fig. 5.8a and Fig 5.8e, showing that the histogram for a two-strip metastable state is comparable to that for the single-strip stable state. For the purpose of identifying transition temperatures at the 10% level, this is an advantageous feature.

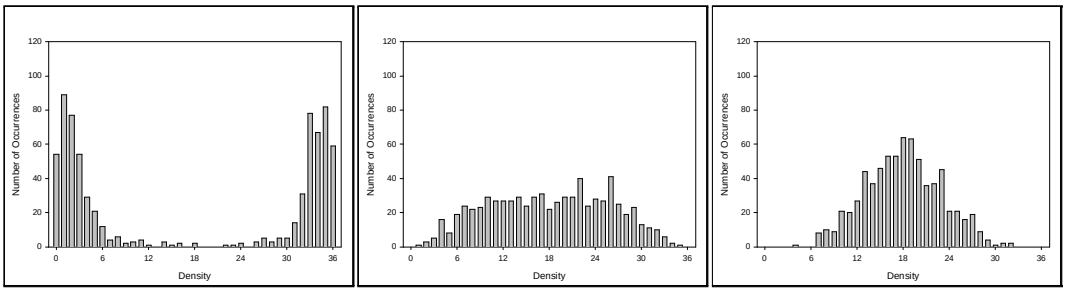

(a) T=1.0 Heating (b) T=1.4 Heating (c) T=2.0

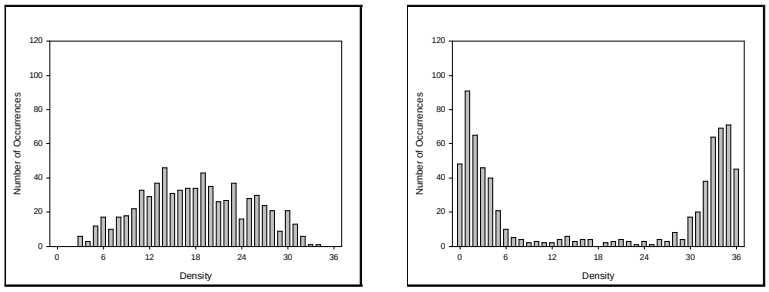

(d) T=1.4 Cooling (e) T=1.0 Cooling

Figure 5.8 Histograms of ρ_0 for $\bar{\rho} = 36/72$, $H = 0$

The histograms for the $\bar{\rho} = 8/72$ system, shown in Figure 5.9, behave in a similar manner. Since there is little difference, except for hysteresis, between heating and cooling cycles, we present only three plots. Corresponding to the ordered state, the distribution is also bimodal but highly asymmetric, since its first moment must be 4 ($\bar{\rho}M$). Similar to the $\bar{\rho} = 36/72$ system, the distribution for a system above criticality appears "normal". Unlike the half filled case,

however, the histogram corresponding to the system undergoing a transition displays a small peak appearing at the high density end. This behavior is typical of a "first order transition" and leads us to the same conclusion drawn from the discontinuity in Fig. 5.7b.

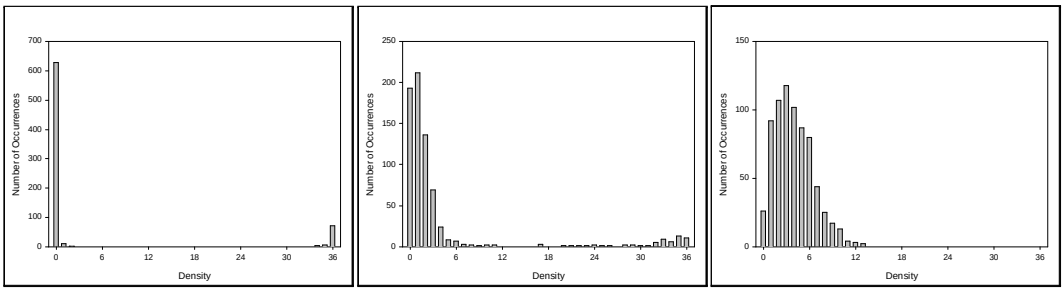

(a) T=0.5 Heating (b) T=0.9 Heating (c) T=1.0 Heating

Figure 5.9 Histograms of column densities for $\overline{\overline{\rho}} = 8/72$, $H = 0$

Histograms clearly carry a wealth of information. However, to be succinct in our determination of transition temperatures, we construct simpler quantities, such as the width of the distribution: (5.3). The dependence of these on T are shown in Figures 5.10a,b. Notice that both plots are very similar to the power plots shown in Figure 5.7a,b. The features of continuous vs. discontinuous transition, as well as hysteresis, are again prominent. We arrive at the same conclusions: $T = 1.3 \pm 0.1$ for $\overline{\rho} = 36/72$ and $T = 0.9 \pm 0.1$ for $\overline{\rho} = 8/72$.

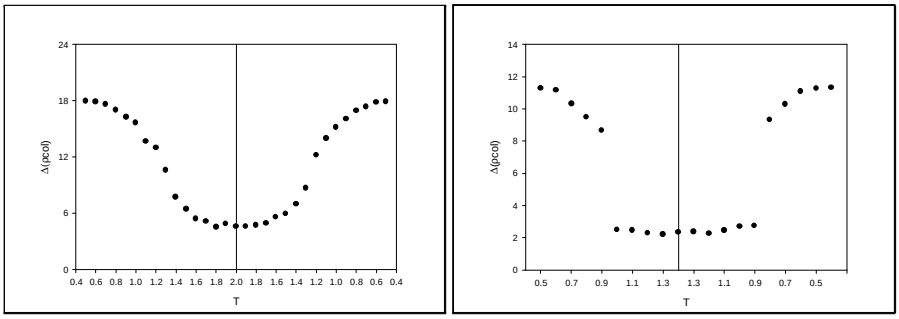

(a) $\bar{\rho} = 36/72$ (b) $\bar{\rho} = 8/72$

Figure 5.10 The dispersion $\Delta\rho_0$ for the (a) $\overline{\rho} = 36/7$ and (b) $8/72$ systems.

As discussed in the previous section, the width $\Delta\rho_h$ is actually measuring different quantities, depending on whether the distribution is bi-modal or single-peaked. To by-pass this difficulty, we turn to "folded" histograms, which are always single-peaked. Other advantages of this construction have been emphasized in the previous section. Figures 5.11a-c are constructed from Figures 5.8a-c.

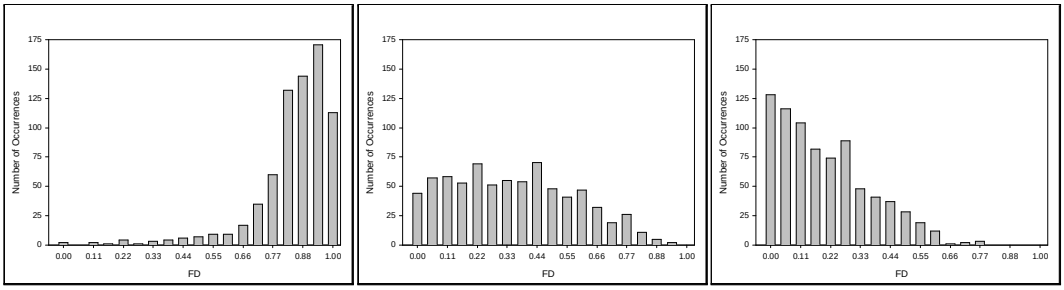

(a) T=1.0 Heating (b) T=1.4 Heating (c) T=2.0

Figure 5.11 "Folded" histograms of column densities for $\bar{\rho} = 36/72$, $H = 0$

Beyond simple folding, we have discussed other subtleties which leads us to create coarse grained figurations before performing the "fold", resulting in much sharper distributions. To see the effects of this operation (5.5), we show the coarse grained version of the configurations of Figs. 5.3 in Figures 5.12a-e.

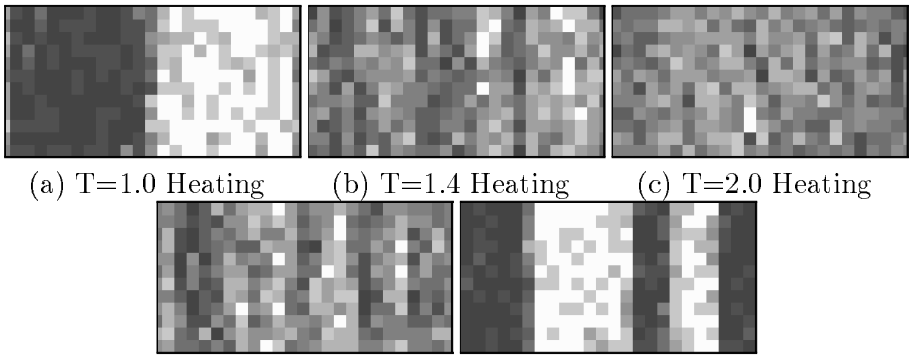

(a) T=1.0 Heating (b) T=1.4 Heating (c) T=2.0 Heating

(d) T=1.4 Cooling (e) T=0.9 Cooling

Figure 5.12 Configurations from Figure 5.3 after coarse graining.

From these coarse grained configurations, we construct the "folded" version of Figures 5.8a-c, displayed in Figures 5.13a-c. As we see, these are sharper than those in Fig. 5.11, so that a better estimate for the transition can be made.

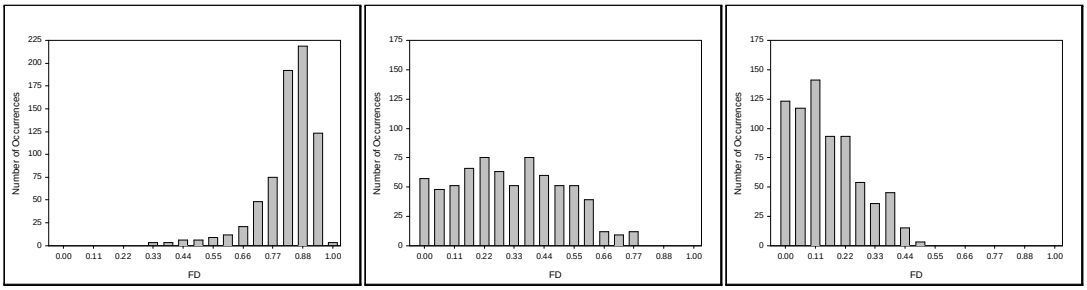

(a) T=1.0 Heating (b) T=1.4 Heating (c) T=2.0

Figure 5.13 "Folded" CG histograms of column densities for $\bar{\rho} = 36/72$, $H = 0$

From these "folded" histograms, we measure the dispersion $\Delta(FD)$ (5.4). Their behavior during the heating and cooling cycles, for both the $\bar{\rho} = 36/72$ and $8/72$ systems, are shown in Figure 5.14.

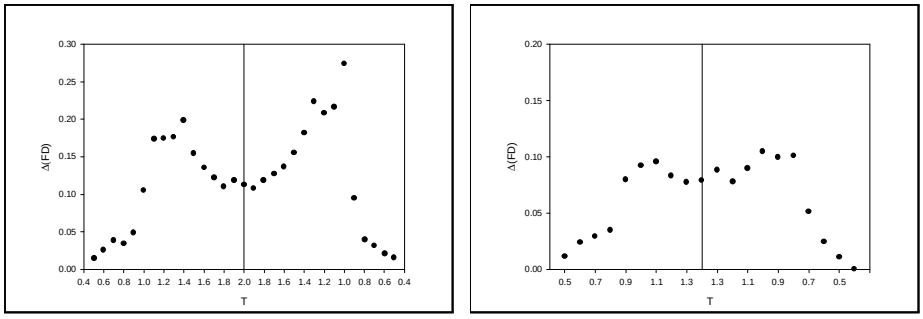

(a) $\bar{\rho}$=36/72 (b) $\bar{\rho}$=8/72

Figure 5.14 The dispersion $\Delta(FD)$ for the (a) $\bar{\rho} = 36/72$ and (b) $8/72$ systems.

The peak of these dispersions are expected at the transition temperatures. We see that this method of identifying the transition is perhaps more reasonable than relying on inflections in $\Delta\rho_0$. Certainly, it leads to results that are entirely consistent with those from analyzing the structure factors.

The third tool involves studying the distributions of *cluster sizes and densities*. Indeed, we will see that a 3-D plot of distribution over the density-temperature variable reveals much of the co-existence curve.

In a series of figures (Figure D.2 in Appendix D), we show the total mass, as a function of the cluster density (ρ_{clus}) and cluster size (V_{clus}), during the heating cycle in the $\bar{\rho} = 36/72$ system. These figures are clearly revealing the drastically different characteristics between an ordered and disordered state. Far below criticality, there is typically one giant cluster with relatively high density. Note that there is a second peak near $(\rho_{clus}, V_{clus}) = (1, 0)$. This is due to the particles in the hole-rich region. As they form small clusters, the densities are close to unity. Of course, there are large numbers of such minute clusters. Had we plotted an ordinary histogram, they would have dominated the picture. This is the crucial reason behind using total mass, i.e., considering a *weighted* histogram, instead. As the temperature increases, this cluster becomes less dense and breaks into smaller clusters, much like what we presented in Chapter 4. It is clear that a major change occurred between $T = 1.3$ and 1.4. In the latter setting, no giant cluster is present. Since this is a system at critical density, so that it can be tuned to the critical point, we could expect a wide range of cluster distributions at that point. As T is increased further above criticality, the clusters become even smaller and, as a result, denser.

From these plots, an interesting composite picture emerges. In Figure D.3, we combined the data for the different temperatures and formed a weighted histogram in the ρ_{clus}-T plane. There is clearly a region where the total mass distribution is zero. The interpretation is that the system gives very little "weight" to this region in the ρ_{clus}-T plane. The boundary for this region is quite sharp and we could readily think of this as the co-existence curve.

Following this line of investigation, we turn to the distributions for a $\overline{\rho} = 8/72$ system. In Figure D.4, we show plots for both the heating and cooling phases. Unlike the previous case, even at low temperatures, there is a sizable mass near $(\rho_{clus}, V_{clus}) = (1, 0)$. This phenomenon can be understood if we keep in mind that the overall densities low, so that the particle rich region is quite small compared to the hole-rich one. As a result, the mass associated with the large (high density) cluster does not overwhelm the small clusters in the hole rich region. As we can see, near $T = 0.9$, the two peaks are of similar height while the large cluster peak has entirely disappeared by $T = 1.0$. Thus, we can safely conclude that a transition occurs at $T = 0.9 \pm 0.1$. Finally, note that while there are differences between the heating and cooling cycles, none are too dramatic to be outside the realms of mild hysteresis and statistical errors.

Finally, in Figure 5.15, we show plots of the cluster sizes as a function of T, during both parts of the cycle in the two systems: $\overline{\rho} = 36/72$ and $8/72$.

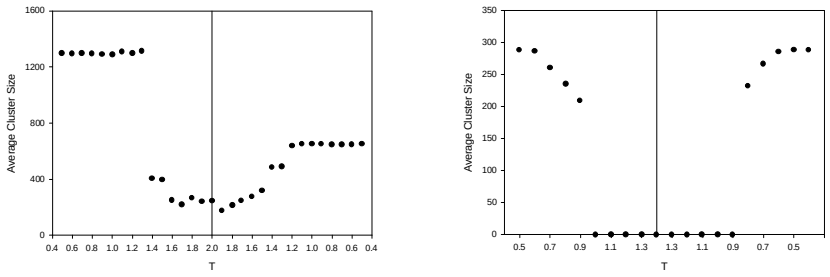

(a) $\bar{\rho}$=36/72 (b) $\bar{\rho}$=8/72

Figure 5.15 Cluster size vs. T for the (a) $\overline{\rho} = 36/72$ and (b) $8/72$ systems.

At first sight, it may be surprising that there is considerable "hysteresis" for a system going through the critical point ($\overline{\rho} = 36/72$). The lower cluster size in the cooling cycle can be traced to the ordering into a metastable state with two strips. This is a compelling reason for studying the density of clusters rather than the sizes. The discontinuity in the heating cycle may be due to the low statistics. Since we took only ten configurations, the effects of critical slowing down may mean that 20K MCS was not enough time for the cluster at $T = 1.3$ to evolve toward a small size. Nevertheless, we believe that we can safely identify the presence of a transition at the level of ± 0.1 in accuracy. For the $\overline{\rho} = 8/72$ system, the discontinuity is most likely a reflection of the nature of the transition being more like a "first order" one.

Lastly, we turn to the measurements of "*internal energy*," which, in our definition, is simply the number of nearest neighbor particle-hole pairs. The maximum for the $\overline{\rho} = 36/72$ system is $2LM = 5184$. However, this is the ordered antiferromagnetic state, corresponding to $T = 0_-$! For the disordered state, it is just 2952. In the $\overline{\rho} = 8/72$ system however, due to the low density, the maximum is just 4 times the number of particles, i.e., 1152. Meanwhile, the minimum for both is just 72, a configuration with a single strip of unit density. With these limits in mind, we consider Figure 5.16a,b, plotting the internal energy for both systems as a function of temperature.

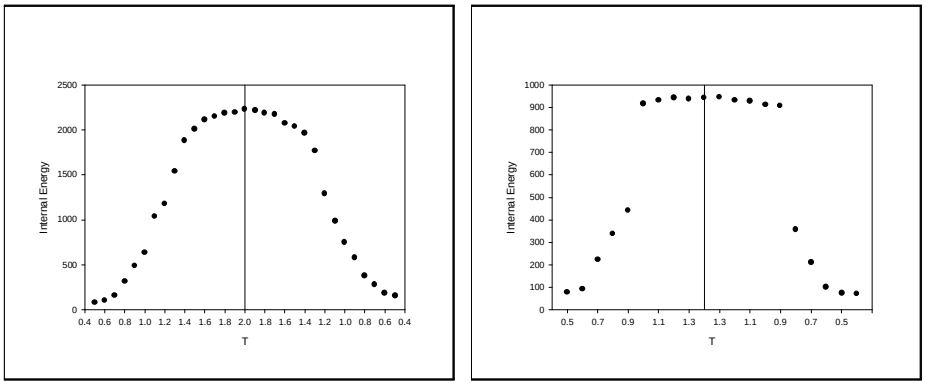

(a) $\bar{\rho}$=36/72 (b) $\bar{\rho}$=8/72

Figure 5.16 Internal energy vs. T for the (a) $\overline{\rho} = 36/72$ and (b) 8/72 systems.

Note that the curve for the half filled system is very similar to that of an equilibrium system, rising from nearly the minimum value of 72 to somewhat below the maximum at $T = 2.0$. During the cooling cycle, the energy does not return to 72. We should expect this behavior, since we know that our system orders into a metastable state with two strips. Thus the ordered state on cooling has nearly twice the internal energy as the initial state. For both systems, these curves confirm the presence of two distinct phases in our system: one associated with high temperatures and the other, with low T. Identifying the transitions by the inflection in one case and the discontinuity in the other case leads us to the conclusions that are completely consistent with the previous ones.

The same techniques presented in detail here are used to estimate the transition temperature for systems ranging from $\rho = 2/72$ to 36/72, at increments of 2/72. For the low densities, all four methods lead to the same transition temperature. At higher densities, there are slight disagreements, which are included as error bars in the estimates.

5.2.1. Systems with varying $\bar{\rho}$ and the coexistence curve for $H = 0$.

In this approach to determine the co-existence curve, we also performed Monte Carlo simulations for systems with *varying* $\bar{\rho}$ and T *held constant*. This method is better suited for estimating the co-existence curve in the region where its slope is far from horizontal. Conversely, where the slopes are too "flat", this method contains large uncertainties. Thus, we concentrated our efforts on estimating the curve away from the "flat" region. Seven temperatures were selected: $0.6 \leq T \leq 1.2$ in 0.1 increments. With fixed T, we start our runs with a random configuration at low desnity: $\bar{\rho} = 4/72$. After evolving for 20K MCS, measurements were taken

and associated with this $(\bar{\rho}, T)$. Then 72 particles are randomly added to the system (so that $\bar{\rho} = 6/72$), evolved another 20K MCS, and measurements taken. This procedure is repeated until $\bar{\rho} = 36/72$, held for an additional 20 K MCS, and then reversed, by stepping the density back down to $\bar{\rho} = 4/72$. These density-increasing and decreasing cycles are analogous to the heating and cooling cycles. For all runs, the four order parameters are used to determine when the system orders. More details of this approach can be found in the discussion of systems with SPBC. Here, we just quote the results in Figure 5.17. The points with vertical error bars are associated with the first approach, using fixed density and varying T. Similarly, the points with horizontal certainties are the results of runs with varying $\overline{\rho}$ and fixed T.

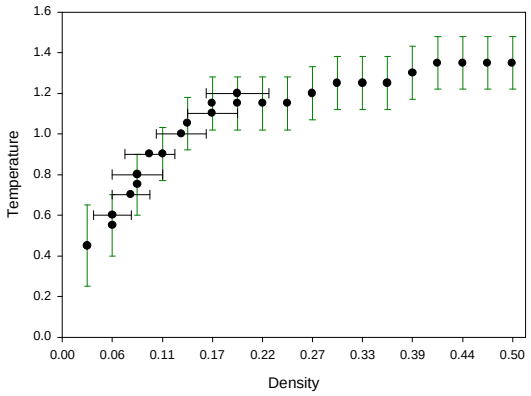

Figure 5.17 Coexistence curve for a system with PBC ($H = 0$).

5.3. Systems with SPBC

In the above analysis we described in detail how we used the order parameters to detect the disorder-order transition for $H = 0$ systems. The same techniques are exploited to investigate systems with SPBC here. Let us emphasize again, SPBC must be included in the definition of, e.g., a cluster and internal energy, so that their measurements include the shift. As a reminder, we use structure factors and column densities that are defined in accordance to the orientation of the bulk. As discussed in Chapter 3, skewed structure factors are appropriate for the low shifts ($H = 3, 4$) and ordinary structure factors for the high shifts ($H = 9, 18$). Similarly, we use skewed column densities(ref 5.2) for the low shifts and ordinary for the high shifts. For each shift, as with the $H = 0$ analysis, we present plots of the order parameters for two systems. Typical configurations are included for the

$\bar{\rho} = 8/72$ system. Chapter 4 includes the typical configurations for the $\bar{\rho} = 36/72$ system.

5.3.1. Two Systems with SPBC(H=3)

Figure 5.18 shows the typical configurations for the $H = 3$ $\bar{\rho} = 8/72$ system. Typical configurations for the $\bar{\rho} = 36/72$ system are given in Figure 4.2. Figures 5.19-5.22 show that the four order parameters give similar results for both systems. The histograms for the vertical (ρ_0) and skewed column density (ρ_h), being similar to the next case, will not be shown.

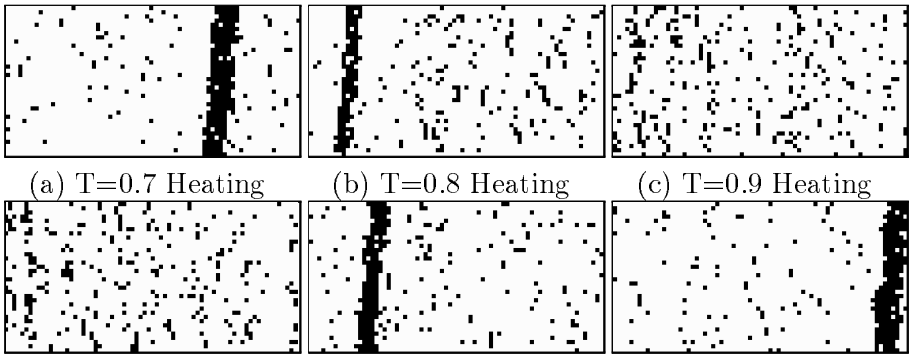

(a) T=0.7 Heating (b) T=0.8 Heating (c) T=0.9 Heating

(d) T=0.9 Cooling (e) T=0.8 Cooling (f) T=0.7 Cooling

Figure 5.18 Typical configurations for $H = 3$, $\bar{\rho} = 8/72$

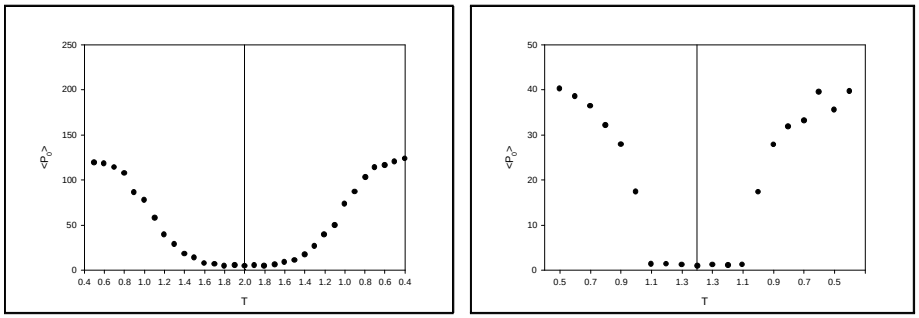

(a) H=3 $\bar{\rho}$ =36/72 (b) H=3 $\bar{\rho}$=8/72

Figure 5.19 The average intensity $< P_0 >$ for the (a) $\bar{\rho} = 36/72$ and (b) 8/72 systems

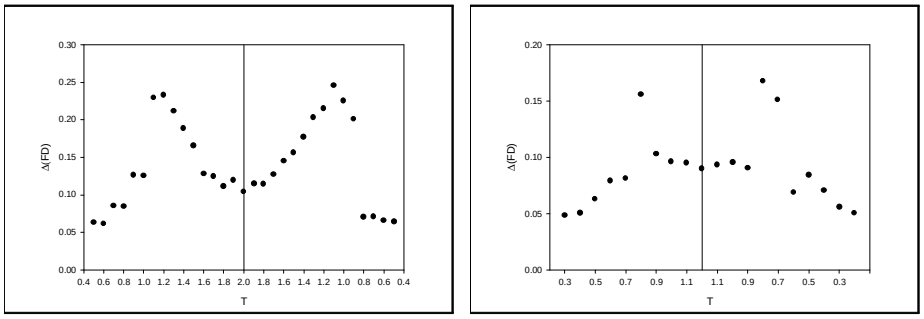

(a) H=3, $\overline{\rho}$ =36/72 (b) H=3, $\overline{\rho}$=8/72

Figure 5.20 The dispersion $\Delta(FD)$ vs. T for the (a) $\bar{\rho} = 36/72$ and (b) 8/72 systems

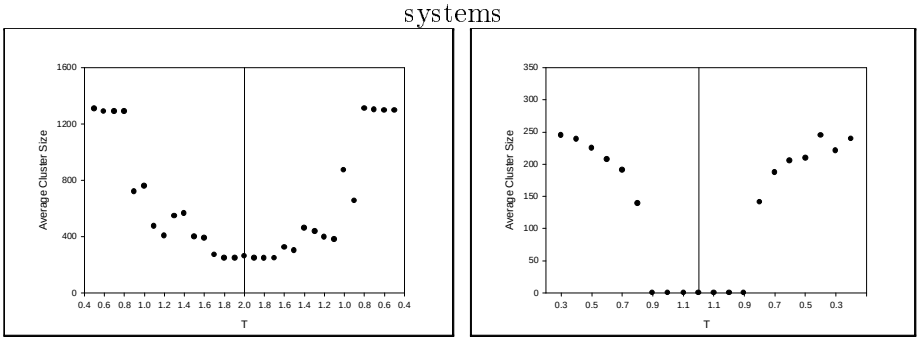

(a) $H = 3, \bar{\rho} = 36/72$ (b) $H = 3, \bar{\rho} = 8/72$

Figure 5.21 Cluster size vs. T for the (a) $\bar{\rho} = 36/72$ and (b) 8/72 systems

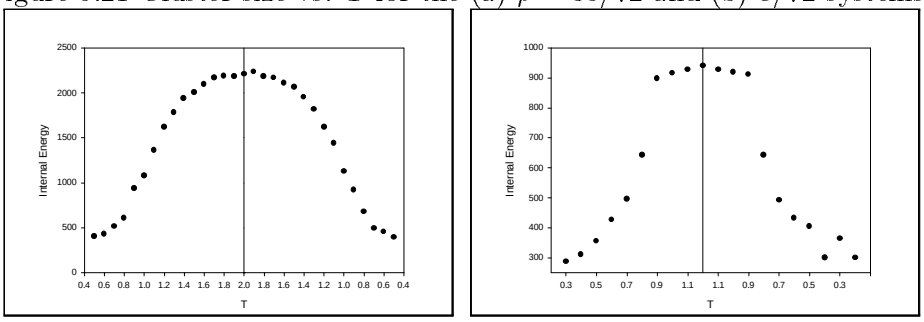

(a) $H = 3, \bar{\rho} = 36/72$ (b) $H = 3, \bar{\rho} = 8/72$

Figure 5.22 The internal energy vs. T for the (a) $\bar{\rho} = 36/72$ and (b) 8/72 systems

5.3.2. Two Systems with SPBC (H=4)

Figure 5.23 shows typical configurations for the $H = 4$ $\bar{\rho} = 8/72$ system. Typical configurations for the $\bar{\rho} = 36/72$ system are given in Figure 4.3. Figures 5.24,5.27-5.29 show that the four order parameters give similar results for both systems.

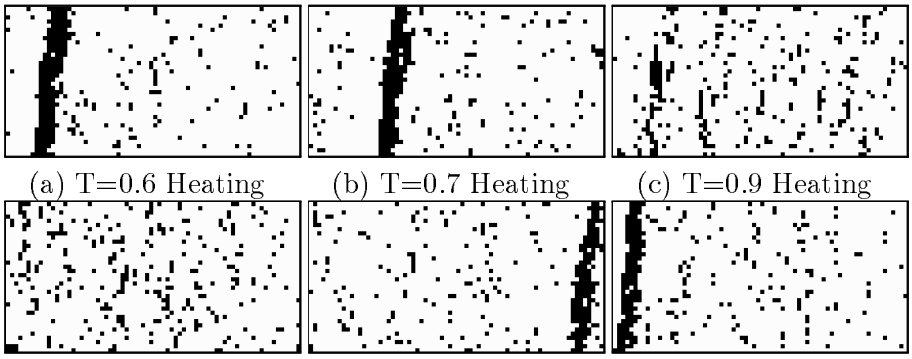

(a) T=0.6 Heating (b) T=0.7 Heating (c) T=0.9 Heating

(d) T=0.8 Cooling (e) T=0.9 Cooling (f) T=0.6 Cooling

Figure (5.23) Typical configurations for $H = 4$, $\bar{\rho} = 8/72$

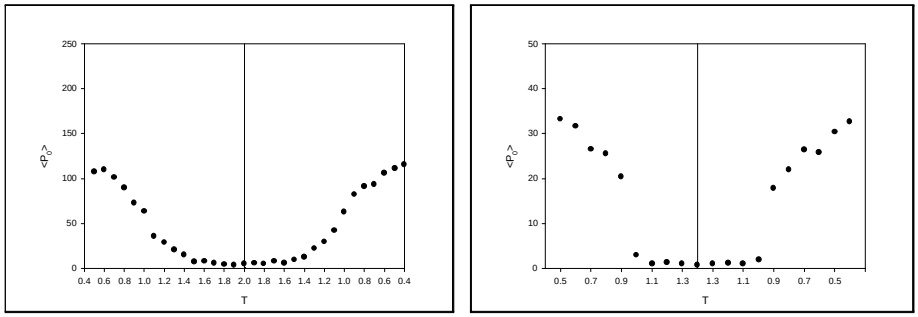

(a) $H = 4$, $\bar{\rho} = 36/72$ (b) $H = 4$, $\bar{\rho} = 8/72$

Figure 5.24 The average intensity $< P_0 >$ for the (a) =36/72 and (b) 8/72 systems

Before we show the $\Delta(FD)$ order parameter for $H = 4$, we compare the vertical (ρ_0) and skewed column density (ρ_H) histograms before folding. Their differences are somewhat greater than the $H = 3$ case, not surprisingly. Thus, we only show them for this case. First, we compare them for the $\bar{\rho} = 36/72$ system. In the ordered state, the histograms for ρ_4 (Figure 5.25d), display slightly sharper bimodal peaks than those for ρ_0 (Figure 5.25a). For the disordered state, histograms are similar as shown in Figure 5.25c,f. Near criticality, the distribution for ρ_0 (Figures 5.25b) extends over the entire range (0-36), whereas the distribution for ρ_4 are somewhat more compact. When *folded*, the two widths differ. Though this difference is small, it is measurable and illustrates our motivation for using ρ_4 for the measuring order in systems with $\bar{\rho} \sim 1/2$.

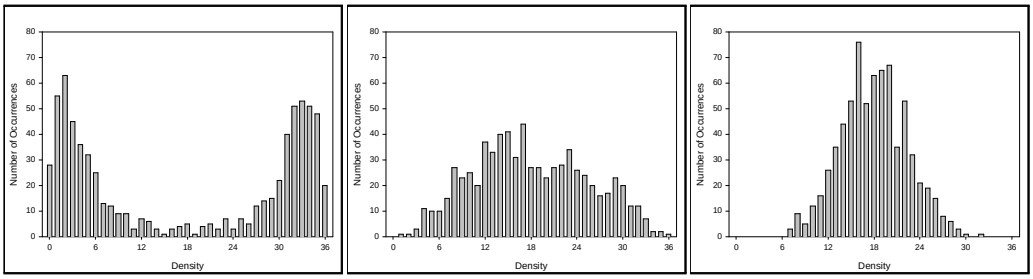

(a) ρ_0 $T = 0.8$ (b) ρ_0 $T = 1.3$ (c) ρ_0 $T = 1.8$

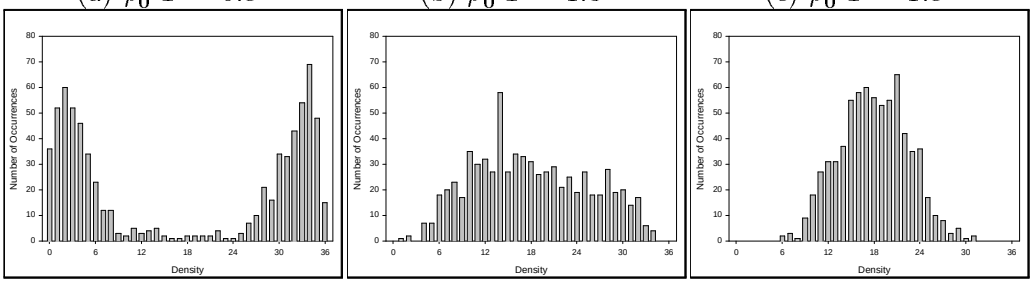

(d) ρ_4 $T = 0.8$ (e) ρ_4 $T = 1.3$ (f) ρ_4 $T = 1.8$

Figure 5.25 Vertical vs. Column Densities $\bar{\rho} = 36/72$

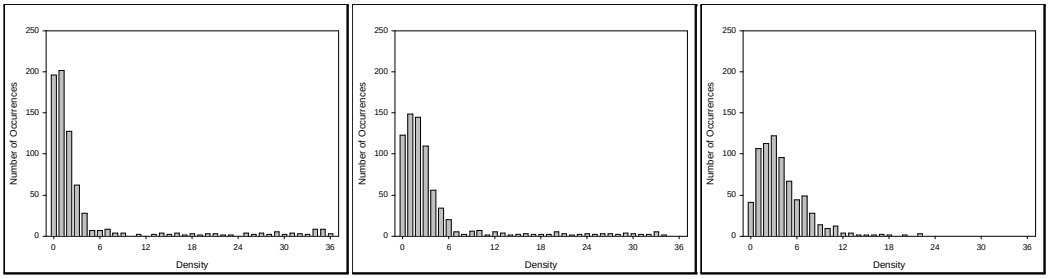

(a) $\rho_0 T = 0.4$ (b) ρ_0 $T = 0.7$ (c) ρ_0 T=0.8

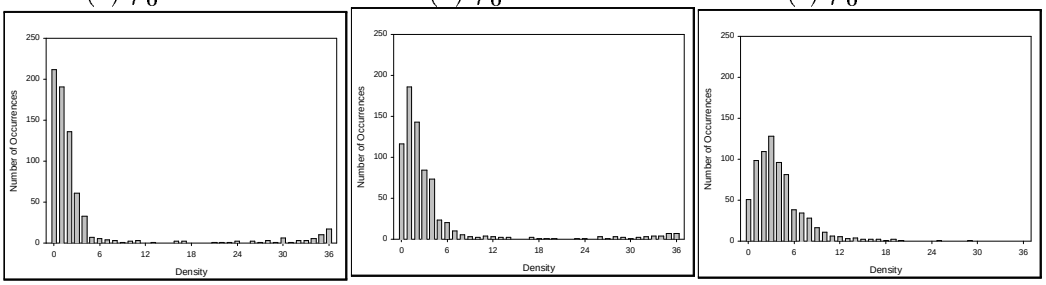

(d) ρ_4 $T = 0.4$ (e) ρ_4 $T = 0.7$ (f) ρ_4 $T = 0.8$

Figure 5.26 Vertical vs.Skewed Column Densities $\bar{\rho}$=8/72

The difference between the two column densities is more clearly seen in the low density, $\bar{\rho} = 8/36$, system. Deep in the ordered phase, the peak at 36 is more pronounced in the ρ_4-distribution (Figure 5.26d), showing that the system is in a single strip state tilted forwards. Even near the transition ($T = 0.7$), the ρ_4-distribution shows some peak at high densities. As with the $\bar{\rho} = 36/72$ system, histograms for the disordered phase are similar (Figure 5.26c,f). Note that, unlike the distributions for the half-filled case, the transition here resembles first order, in that a second peak develops far from the dominant one.

Below, we show the widths associated with the *folded* ρ_4 histograms, $\Delta(FD)$, because it provides a better estimate for the transition temperature in systems with low shifts and low densities (Figure 5.27). Also, as in the previous cases, average cluster size and internal energies are also displayed (Figures 5.28 and 5.29).

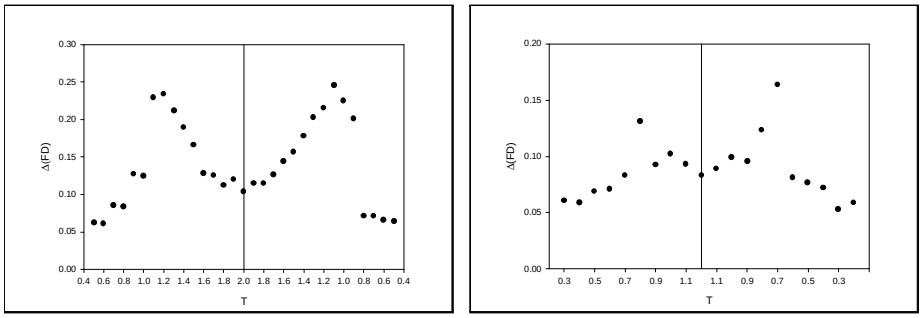

(a) $H = 4$, $\overline{\rho} = 36/72$ (b) $H = 4$, $\overline{\rho} = 8/72$

Figure 5.27 The dispersion $\Delta(FD)$ vs. T for the (a) $\bar{\rho} = 36/72$ and (b) 8/72 systems

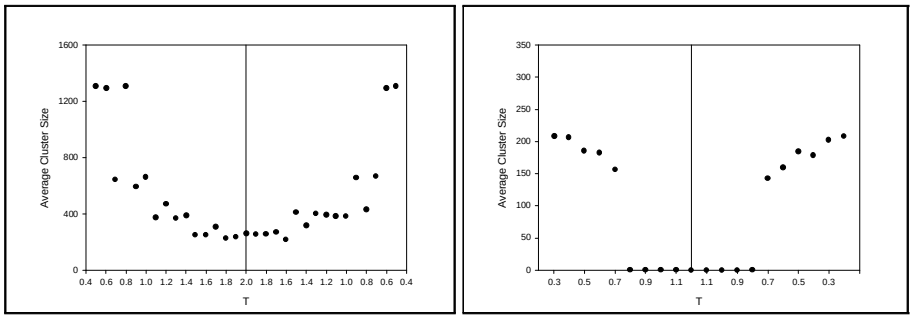

(c) $H = 4$, $\bar{\rho} = 36/72$ (d) $H = 4, \bar{\rho} = 8/72$

Figure 5.28 Cluster size vs. T for the (a) $\bar{\rho} = 36/72$ and (b) 8/72 systems

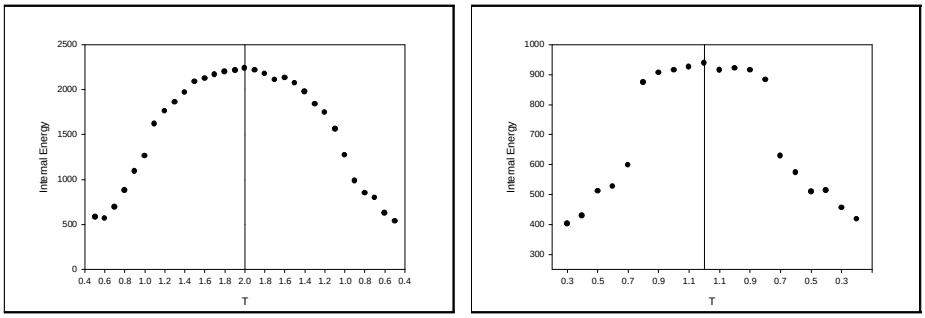

(a) $H = 4$, $\bar{\rho} = 36/72$ (b) $H = 4$, $\bar{\rho} = 8/72$

Figure 5.29 Internal energy vs. T for the (a) $\bar{\rho} = 36/72$ and (b) $8/72$ systems

5.3.3. Two Systems with SPBC (H=9)

Figure 5.30 shows typical configurations for the $H = 9$, $\bar{\rho} = 8/72$ system. Again, typical configurations for the $\bar{\rho} = 36/72$ case are to be found in Chapter 4 (Figure 4.4). Unlike for systems with low shifts, here we use the dispersion $\Delta\rho_0$ as the order parameter for column densities and not $\Delta(FD)$. The disadvantage of the latter lies in finite size effects and interface fluctuations. As discussed in Chapter 4, the ordered state for a high $\bar{\rho}$, $H = 9$ system consists of a narrow strip with multiple windings, so that there are many interfaces. Neither aspects are favored by the inter-particle attraction, leading to strip-merging and large fluctuations in the column densities even in the inhomogeneous state. Thus, the distributions of a folded histogram is just as broad as the unfolded case, so that we resort to the more "primitive" $\Delta\rho_0$.

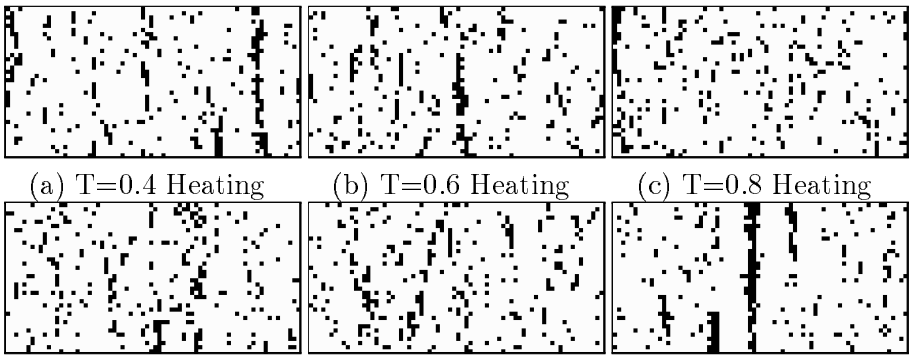

(a) T=0.4 Heating (b) T=0.6 Heating (c) T=0.8 Heating

(d) T=0.8 Cooling (e) T=0.6 Cooling (e) T=0.4 Cooling

Figure 5.30 Typical configurations for $H = 9$, $\bar{\rho} = 8/72$

Figures 5.31-5.34 show that all four order parameters (average intensity $< P_0 >$, $\Delta\rho_0$, average cluster size, and internal energy) provide a consistent picture for either system. Note that the average cluster size seems to show a discontinuity even for the half-filled case. Meanwhile, the internal energy measurements for the =8/72 system seem smoother than the other order parameters. These aspects are not well understood. They may be due to the small sample of configurations used and/or that the clusters have four surfaces and not two as in PBC.

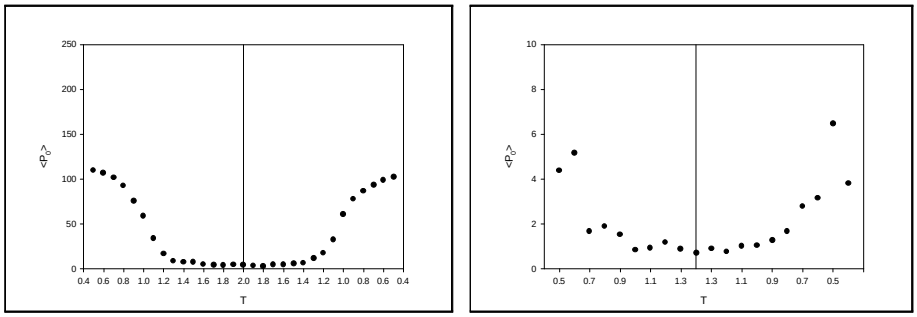

(e) $H = 9$, $\bar{\rho} = 36/72$ (f) $H = 9$, $\bar{\rho} = 8/72$

Figure 5.31 The average intensity $< P_0 >$ for the (a) =36/72 and (b) 8/72 systems

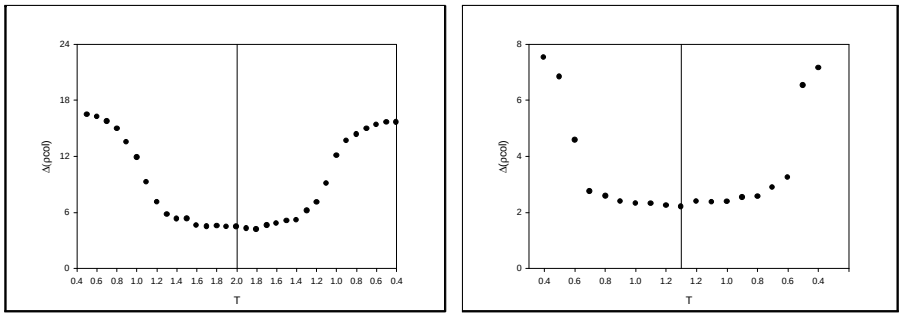

(a) $H = 9$, $\bar{\rho} = 36/72$ (b) $H = 9$, $\bar{\rho} = 8/72$

Figure 5.32 The dispersion $\Delta\rho_0$ vs. T for the (a) $\bar{\rho} = 36/72$ and (b) 8/72 systems

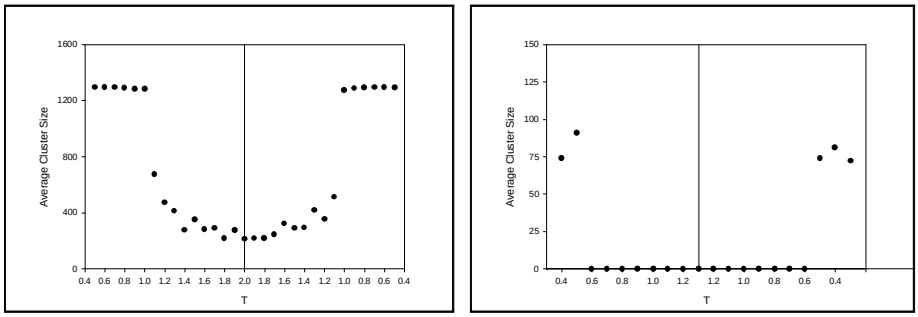

(e) $H = 9$, $\bar{\rho} = 36/72$ (f) $H = 9$, $\bar{\rho} = 8/72$

Figure 5.33 Cluster size vs. T for the (a) $\bar{\rho} = 36/72$ and (b) $8/72$ systems

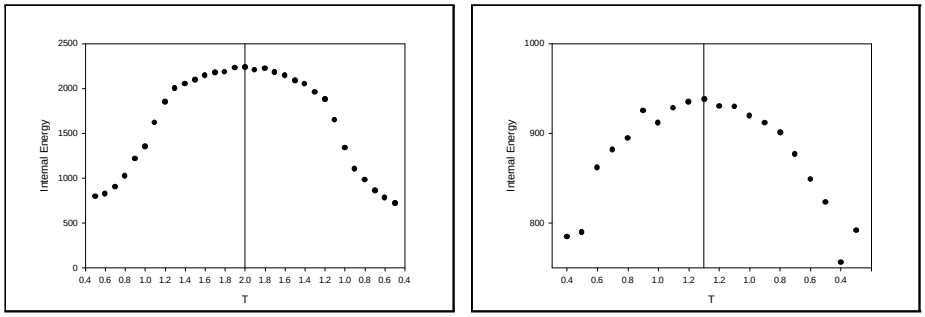

(a) $H = 9$, $\bar{\rho} = 36/72$ (b) $H = 9$, $\bar{\rho} = 8/72$

Figure 5.34 Internal energy vs. T for the (a) $\bar{\rho} = 36/72$ and (b) $8/72$ systems

5.3.4. Two Systems with SPBC (H=18)

Figure 5.35 shows typical configurations for the $H = 18$, $\bar{\rho} = 8/72$ system. Typical configurations for the half-filled case are given in Figure 4.5. As with $H = 9$, we use the $\Delta\rho_0$ as the order parameter for column densities instead of $\Delta(FD)$. Figures 5.36-5.39 show that the four order parameters give consistent results for both the high and low density systems. In contrast to $H = 9$, the wider strips here are less susceptible to the interface fluctuations, so that strip merging is less likely. Notice that this state is stable at temperatures as high as *T=1.3* (Figure 4.4c,d). At this high shift, the identification of a transition temperature is again much easier, as we can see from the abrupt changes of behavior in all quantities, including $< P_0 >$.

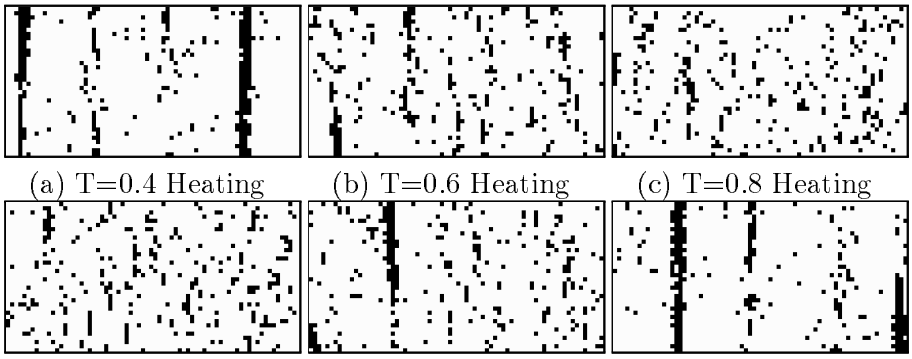

(a) T=0.4 Heating (b) T=0.6 Heating (c) T=0.8 Heating

(d) T=0.8 Cooling (e) T=0.6 Cooling (f) T=0.4 Cooling

Figure 5.35 Typical configurations for $H = 18$, $\bar{\rho} = 8/72$

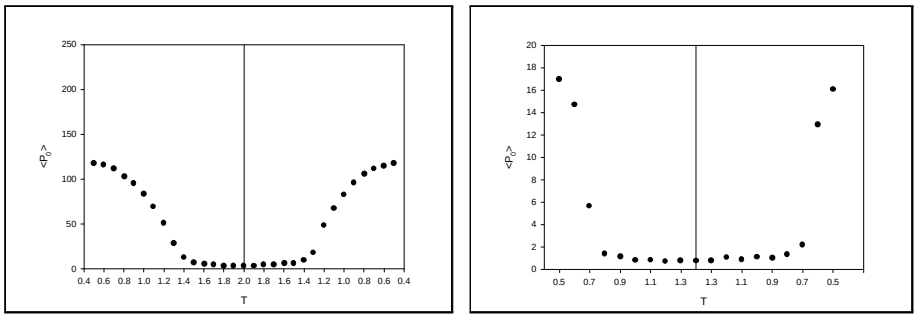

(g) $H = 18, \bar{\rho} = 36/72$ (h) $H = 18$, $\bar{\rho} = 8/72$

Figure 5.36 The average intensity $< P_0 >$ for the (a) =36/72 and (b) 8/72 systems

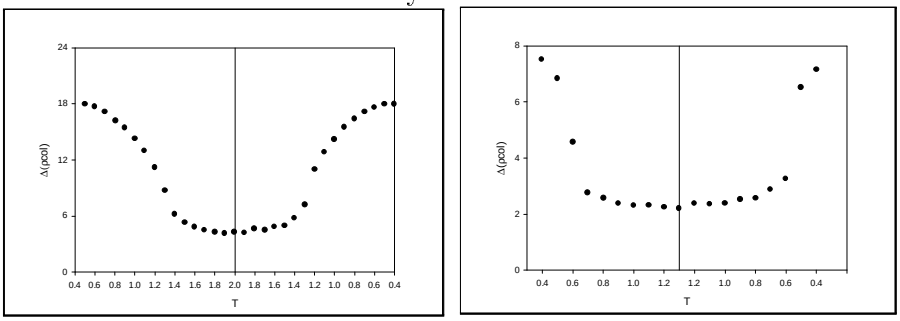

(a) $H = 18$, $\bar{\rho} = 36/72$ (b) $H = 18$, $\bar{\rho} = 8/72$

Figure 5.37 The dispersion $\Delta\rho_0$ vs. T for the (a) $\bar{\rho} = 36/72$ and (b) 8/72 systems

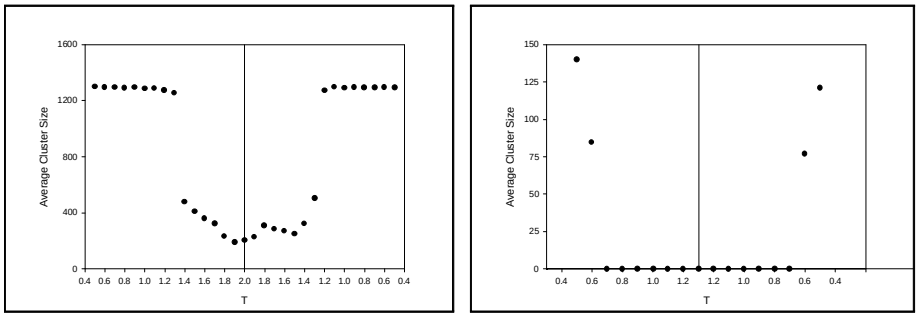

(g) $H = 18$, $\bar{\rho} = 36/72$ (h) $H = 18$, $\bar{\rho} = 8/72$

Figure 5.38 Cluster size vs. T for the (a) $\bar{\rho} = 36/72$ and (b) $8/72$ systems

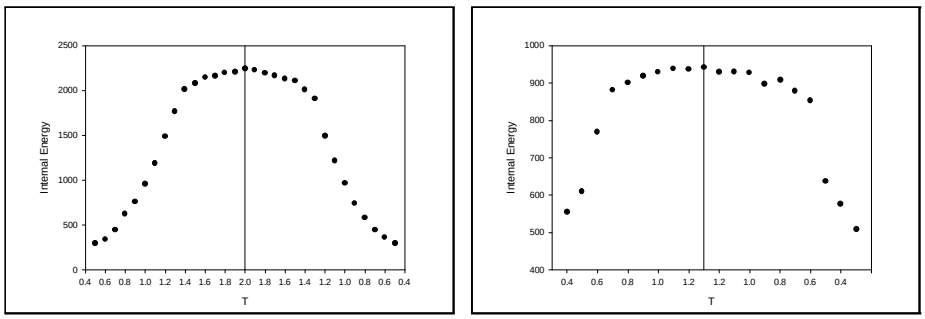

(a) $H = 18$, $\bar{\rho} = 36/72$ (b) $H = 18$, $\bar{\rho} = 8/72$

Figure 5.39 Internal energy vs. T for the (a) $\bar{\rho} = 36/72$ and (b) $8/72$ systems

5.3.5. Systems with varying $\bar{\rho}$.

As in the study of systems with PBC, we also performed Monte Carlo simulations for systems with varying $\bar{\rho}$ and fixed T. As this method is more suited for estimating the coexistence curve with a large slope, we concentrated our efforts on estimating the curve away from the "flat" region. Unlike the constant T study, we use only column density to establish ordering. Here, we only show a few column density histograms at one temperature ($T = 0.8$) to illustrate how we established the co-existence curve. We include the PBC case here as reference: Figure 5.40. It shows the distribution is single peaked at $\rho = 6/72$, but bi-modal at $\rho = 8/72$, so that a reasonable estimate of the critical density for the $H = 0$ system is $\rho = 7/72 \pm 1/72$.

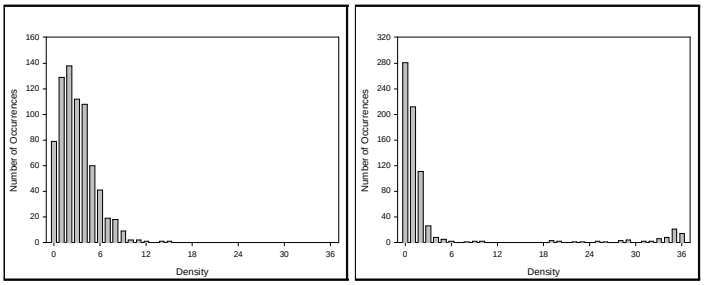

(a) ρ_0 for H=0, $\bar{\rho}$=6/72 (b) ρ_0 for H=0, $\bar{\rho}$=8/72

Figure 5.40 Column density histograms at $T = 0.8$ for $H = 0$

Proceeding to the systems with SPBC, we only show two shifts: $H = 4, 18$. In the former case (Figure 5.41), we see again that the skewed column density ρ_4 is better at indicating ordering than ρ_0. From this figure, we estimate the critical density to be $\rho = 9/72 \pm 1/72$. For the $H = 18$ system, the opposite is true and we show, in Figure 5.42, only two histograms for ρ_0. The transition is less clear and we estimate the critical density to be $\rho = 11/72 \pm 1/72$. These few histograms clearly illustrates that tendency for the shift lower the co-existence curve relative to the curve for the PBC case.

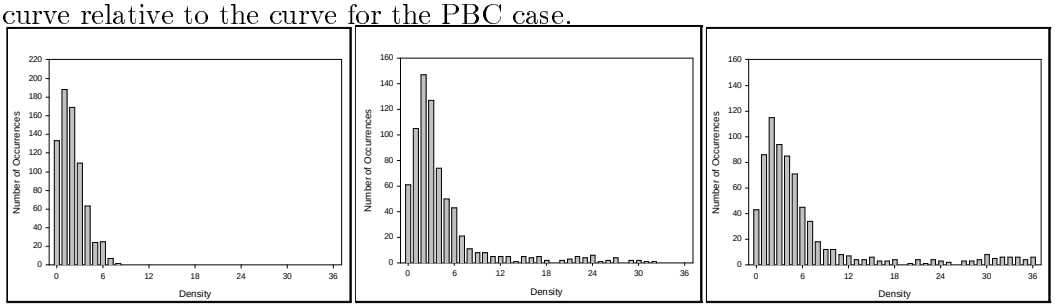

(a) Vertical $\bar{\rho}$=4/72 (b) H=4 Vertical $\bar{\rho}$=9/72 (c) Vertical $\bar{\rho}$=13/72

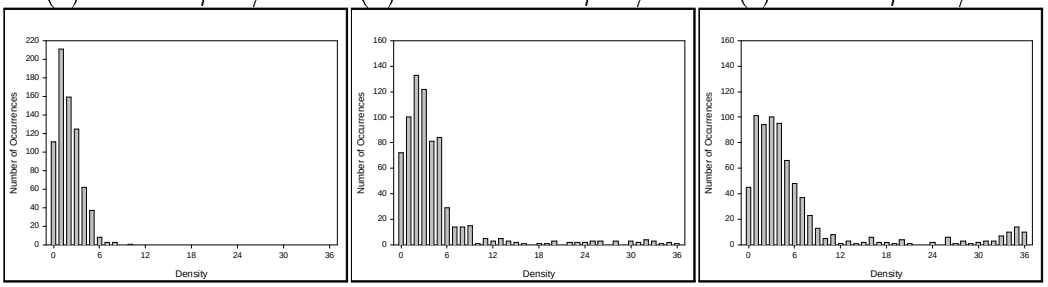

(d) ρ_4 for $\bar{\rho} = 4/72$ (e) ρ_4 for $\bar{\rho} = 9/72$ (f) ρ_4 for $\bar{\rho} = 13/72$

Figure 5.41 Column density histograms at $T = 0.8$ for $H = 4$